



HAL
open science

Chemical kinetics and density measurements of OH in an atmospheric pressure He + O₂ + H₂O radiofrequency plasma

Alexandra Brisset, Andrew Gibson, Sandra Schröter, Kari Niemi, Jean-Paul Booth, Timo Gans, Deborah O'Connell, Erik Wagenaars

► **To cite this version:**

Alexandra Brisset, Andrew Gibson, Sandra Schröter, Kari Niemi, Jean-Paul Booth, et al.. Chemical kinetics and density measurements of OH in an atmospheric pressure He + O₂ + H₂O radiofrequency plasma. *Journal of Physics D: Applied Physics*, 2021, 54 (28), pp.285201. 10.1088/1361-6463/abefec . hal-03200547

HAL Id: hal-03200547

<https://hal.science/hal-03200547>

Submitted on 4 May 2021

HAL is a multi-disciplinary open access archive for the deposit and dissemination of scientific research documents, whether they are published or not. The documents may come from teaching and research institutions in France or abroad, or from public or private research centers.

L'archive ouverte pluridisciplinaire **HAL**, est destinée au dépôt et à la diffusion de documents scientifiques de niveau recherche, publiés ou non, émanant des établissements d'enseignement et de recherche français ou étrangers, des laboratoires publics ou privés.

PAPER • OPEN ACCESS

Chemical kinetics and density measurements of OH in an atmospheric pressure He + O₂ + H₂O radiofrequency plasma

To cite this article: Alexandra Brisset *et al* 2021 *J. Phys. D: Appl. Phys.* **54** 285201

View the [article online](#) for updates and enhancements.



IOP | ebooks™

Bringing together innovative digital publishing with leading authors from the global scientific community.

Start exploring the collection—download the first chapter of every title for free.

Chemical kinetics and density measurements of OH in an atmospheric pressure He + O₂ + H₂O radiofrequency plasma

Alexandra Brisset^{1,*} , Andrew R Gibson^{2,3} , Sandra Schröter¹ , Kari Niemi¹ , Jean-Paul Booth⁴ , Timo Gans^{1,5} , Deborah O'Connell^{1,5}  and Erik Wagenaars¹ 

¹ York Plasma Institute, Department of Physics, University of York, York YO10 5DD, United Kingdom

² Research Group for Biomedical Plasma Technology, Ruhr-Universität Bochum, Universitätsstraße 150, 44801 Bochum, Germany

³ Institute of Electrical Engineering and Plasma Technology, Ruhr-Universität Bochum, Universitätsstraße 150, 44801 Bochum, Germany

⁴ LPP, CNRS, Ecole Polytechnique, UPMC University Paris-Sud, Observatoire de Paris, Université Paris-Saclay, Sorbonne Universités, PSL Research University, 91128 Palaiseau, France

⁵ School of Physical Sciences, National Centre for Plasma Science and Technology, Dublin City University, Dublin 9, Ireland

E-mail: alexandra.brisset@york.ac.uk

Received 2 January 2021, revised 26 February 2021

Accepted for publication 18 March 2021

Published 4 May 2021



Abstract

This work presents experiments and modelling of OH densities in a radio-frequency driven atmospheric-pressure plasma in a plane-parallel geometry, operated in helium with small admixtures of oxygen and water vapour (He + O₂ + H₂O). The density of OH is measured under a wide range of conditions by absorption spectroscopy, using an ultra-stable laser-driven broad-band light source. These measurements are compared with 0D plasma chemical kinetics simulations adapted for high levels of O₂ (1%). Without O₂ admixture, the measured density of OH increases from 1.0×10^{14} to 4.0×10^{14} cm⁻³ for H₂O admixtures from 0.05% to 1%. The density of atomic oxygen is about 1×10^{13} cm⁻³ and grows with humidity content. With O₂ admixture, the OH density stays relatively constant, showing only a small maximum at 0.1% O₂. The simulations predict that the atomic oxygen density is strongly increased by O₂ addition. It reaches $\sim 10^{15}$ cm⁻³ without humidity, but is limited to $\sim 10^{14}$ cm⁻³ beyond 0.05% water content. The addition of O₂ has a weak effect on the OH density because, while atomic oxygen becomes a dominant precursor for the formation of OH, it makes a nearly equal contribution to the loss processes of OH. The small increase in the density of OH with the addition of O₂ is instead due to reaction pathways involving increased production of HO₂ and O₃. The simulations show that the densities of OH, O and O₃ can be tailored relatively independently over a wide range of conditions. The densities of O and O₃ are strongly affected by the presence

* Author to whom any correspondence should be addressed.



Original content from this work may be used under the terms of the [Creative Commons Attribution 4.0 licence](https://creativecommons.org/licenses/by/4.0/). Any further distribution of this work must maintain attribution to the author(s) and the title of the work, journal citation and DOI.

of small quantities (0.05%) of water vapour, but further water addition has little effect. Therefore, a greater range and control of the reactive species mix from the plasma can be obtained by the use of well-controlled multiple gas admixtures, instead of relying on ambient air mixing.

Keywords: atmospheric pressure radiofrequency discharge, absorption spectroscopy, plasma chemistry, modelling

(Some figures may appear in colour only in the online journal)

1. Introduction

Non-equilibrium atmospheric-pressure plasmas are known to be efficient sources of reactive species [1–13] and have been investigated for several different applications, in particular surface processing, environmental applications and plasma medicine [7, 14–34]. One of the challenges is tailoring the plasma gas-phase chemistry to each specific application. Tailoring the chemistry is usually achieved by adjusting external parameters such as: the gas composition [6, 7, 14–16], the electric field distribution (by modifying the source design), or the applied voltage characteristics (direct or pulsed voltage, rise time, amplitude, frequency) [17, 18, 35–37]. The latter two approaches can require modification of the plasma hardware, limiting their value for process control and operation for multiple different processes. Modifying the gas composition generally provides the most operational flexibility. Atmospheric pressure plasmas generally operate in rare gases with complex admixtures, arising from deliberate molecular gas additions, ambient air entrainment and/or impurities. The full plasma chemistry needs to be understood in order to effectively manipulate the density of desired reactive species.

For biomedical applications the emphasis has been on understanding and optimising the production of reactive oxygen and nitrogen species due to their high oxidative power and their natural roles in major biological functions (in particular in the immune system, or as signalling molecules in cellular functions [1, 3, 4, 16, 23, 24]). In the presence of water, which can come from the biological target, itself or may be intentionally introduced to the feed gas, hydrogen peroxide (H_2O_2) attracts particular attention. It is a relatively long-lived and powerful oxidising species that can interact with distant targets, and can be generated in significant concentrations [3, 38, 39]. One of the main mechanisms for the production of hydrogen peroxide in plasmas is the three-body recombination of two hydroxyl (OH) radicals. Therefore, understanding the production and destruction pathways of hydroxyl radicals is necessary to optimise and control hydrogen peroxide for applications.

Molecular oxygen (O_2) is often added to the gas mixture to produce O-based reactive species such as atomic oxygen and ozone, which also play important roles in disinfection and oxidation. Ozone is used in a wide range of applications, including treatment of municipal and waste water, and for food processing [5, 8, 9, 40]. It is a powerful germicide and also efficiently neutralises organic odours. In the context of complex

admixtures, the control of both OH/ H_2O_2 and O/ O_3 is important. RF plasma sources in He + O_2 + H_2O mixtures (the focus of this paper) are excellent sources of both H-species and O-species, and some tailoring of gas chemistry has been demonstrated. Several studies have investigated how changing the gas composition allows optimisation for a given application [14, 41]. In particular, numerical simulations have elucidated the effect of either oxygen or water vapour addition on the generation of the ROS, and the relative contribution of different production and loss reactions.

These studies have helped to begin unravelling the mechanisms of ROS formation and their interaction with biological samples. The production of O-based species is greatly enhanced by the addition of O_2 to the gas mixture, due to additional reaction pathways. Conversely, the addition of water vapour to a discharge already containing O_2 appears to hinder the production of O-based species. On the other hand, the addition of both water and of O_2 increases the density of H-containing species [14, 41–43]. Therefore, the ROS composition in the gas phase can be controlled by varying the gas mixture. Remarkably, the total ROS concentration was observed to be little changed when the ratio $[\text{H}_2\text{O}]/[\text{O}_2]$ was varied over four orders of magnitude (for similar dissipated energies) [41]. This is despite dramatic changes in the dominant chemical reactions, indicating that both O_2 and H_2O are efficient additives for ROS production.

In the specific case of hydroxyl, it was shown that its density mostly depends on the concentration of water vapour, and is relatively insensitive to O_2 addition (over the range of 0.1%–1% of O_2). However, the dominant reactions for both production and loss change dramatically in the presence of O_2 [14]. In more detail, when only water is present, OH is mostly produced by electron impact dissociation of H_2O and lost by recombination of two OH radicals in a three-body process. In the presence of oxygen, the dominant OH production and loss reactions are driven by $\text{O}(^1\text{D})$ and O, respectively. Under these conditions, the net contribution of oxygen to the formation of OH (as defined below) is not clear, since both production and loss pathways are enhanced. In the presence of high concentrations of water vapour, the complex role of lower density secondary species needs to be identified in more detail in order to fully understand the plasma chemistry. Such secondary species (for example, HO_2) are formed through two-step (or more) processes, and generally have low densities for low water vapour concentration, but start to significantly affect the kinetics at high water concentrations. In the literature, studies

usually present the percentage contribution of individual reactions towards the production (or loss) of hydroxyl relative to the total production (or loss) rate. This enables the dominant reactions for production and loss to be determined. However, this representation does not show the net contribution of a given species to the generation of hydroxyl, i.e. the effective contribution of a given species, or group of species, to the total production rate of hydroxyl, defined as the rate of production of hydroxyl from reactions of the given species minus the rate of loss of hydroxyl in collisions with that species. In this paper, an analysis of the reaction rates is used to identify the net contribution of each given species. A detailed analysis of the kinetics of the generation of OH and other ROS is performed for a range of admixture ratios $[O_2]/[H_2O]$.

The previous studies cited above present simulations, whereas this paper presents new experimental data, expanding on the limited experimental results that can be found in the literature [9, 44–48]. The OH densities were measured for various concentrations of O_2 and H_2O , up to 1% in each case. They were obtained using a broad-band UV-absorption spectroscopy technique using an ultra-stable broad-band light source [47, 49]. This light source has excellent temporal intensity stability, leading to an absorption baseline variability lower than 2×10^{-5} over the range of the $OH(X) \rightarrow OH(A)$ transition (306–311 nm) [49]. This setup allows a detection limit one order of magnitude lower compared to the typical limit (about 10^{-3}) that can be achieved with the more commonly used UV-LEDs [9].

2. Experimental setup and modelling

2.1. Plasma source

The RF-driven plasma source used here was described in detail in [5] and is illustrated in figure 1. Briefly, a quasi-homogenous plasma is generated between two plane-parallel electrodes with a 1 mm gap. The length of the electrodes is 30 mm and the width is 10 mm offering a surface-to-volume ratio of 2 mm^{-1} . Two MgF_2 windows close the reactor in the direction perpendicular to the plane electrodes. An RF generator (Coaxial-Power, MN 150-13.56) and an L-matching network (Coaxial-Power, MMN 150) are used to drive the discharge at a frequency of 13.56 MHz and a dissipated power of $15.0 \pm 1.5 \text{ W cm}^{-3}$. Voltage and current are measured with a PMK-14KVAC Tektronix probe (1000:1) and an Ion Physics Corp. CM-100 I probe (1 V A^{-1}) from which the dissipated power was calculated following the method of [50].

The total gas flow is 5 slm. Helium with a purity of 99.996% was used. Most of the gas lines are made of stainless-steel to limit the impurities in the gas. Water vapour and oxygen are admixed to the gas flow using three mass flow controllers. A defined content of water vapour is added to the feed gas by guiding a fraction of the total helium flow through a glass bubbler filled with distilled water. The amount of water vapour is calculated using the vapour pressure at room temperature and the flow rate through the bubbler as in [47]. The output gas of the reactor is guided to an exhaust several meters downstream.

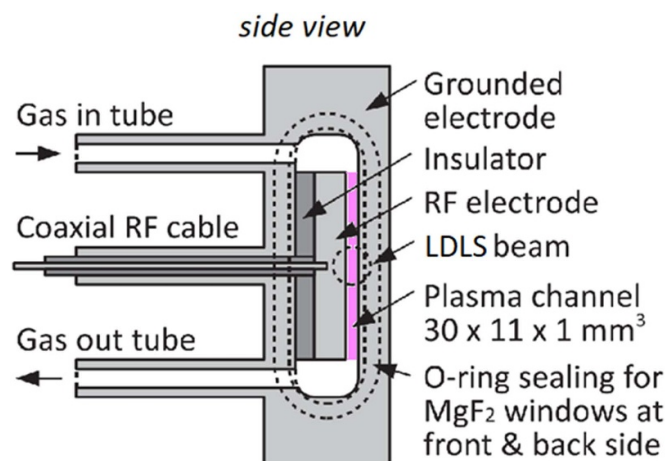


Figure 1. Schematic cross section of the plasma source. The light source section is represented by the single round dashed line. It is centred at 1.5 cm of the plasma channel. RF: radio frequency, LDLS: laser driven light source. Reprinted from [5], with the permission of AIP Publishing.

2.2. Absorption spectroscopy

The hydroxyl densities are measured by absorption spectroscopy using an ultra-stable laser-driven broad-band light source (LDLS, Energetiq EQ-99) and reflective optics to limit chromatic aberrations (figure 2). The divergent light coming out of the light source is focused into the central plane of the discharge, collected and focussed onto the spectrograph's entrance slit by four parabolic mirrors (UV enhanced aluminium MPD-F01 Thorlabs). The focal beam waist is about 2 mm, so that the measured density of hydroxyl is spatially averaged over the 1 mm gap between the electrodes. The optical absorption path of 11 mm comprises the width of the electrodes and both 0.5 mm gaps between windows and electrodes. This path is perpendicular to the feed gas flow. The transmitted spectrum is recorded by a 0.5 m Czerny–Turner spectrograph (Andor SR500i) equipped with a 2400 l mm^{-1} grating that is blazed for $\lambda = 300 \text{ nm}$ and a CCD camera (Andor, Newton DU940P-BU2, 2048×512 pixels of $13.5 \times 13.5 \mu\text{m}^2$ size). The spectrometer entrance slit width was set to $100 \mu\text{m}$, resulting in an instrumental broadening of 0.03 nm (see figure 3). Additional apertures in the beam path were used to reduce unnecessary optical plasma emission reaching the entrance slit. The OH ground state density is determined from the intensity of the integrated $OH(X^2\Pi_i, \nu'' = 0) \rightarrow OH(A^2\Sigma^+, \nu' = 0)$ rotational envelope in the wavelength range 306–310 nm.

As previously described in several papers [9, 47, 49], the absolute density of the hydroxyl radical, n_{OH} , is obtained from analysis of the measured plasma absorbance spectrum $A(\lambda)$ in the spectral range from 306 to 311 nm, assuming the Beer–Lambert law (equations (1) and (2)). Four signals are measured successively to correct for background and plasma emission. The first signal is recorded with both the plasma and the light source on (S_{PL}), the second records the intensity of the light source only (S_L), the third records the plasma emission only (S_P) and the last signal is a background with both plasma

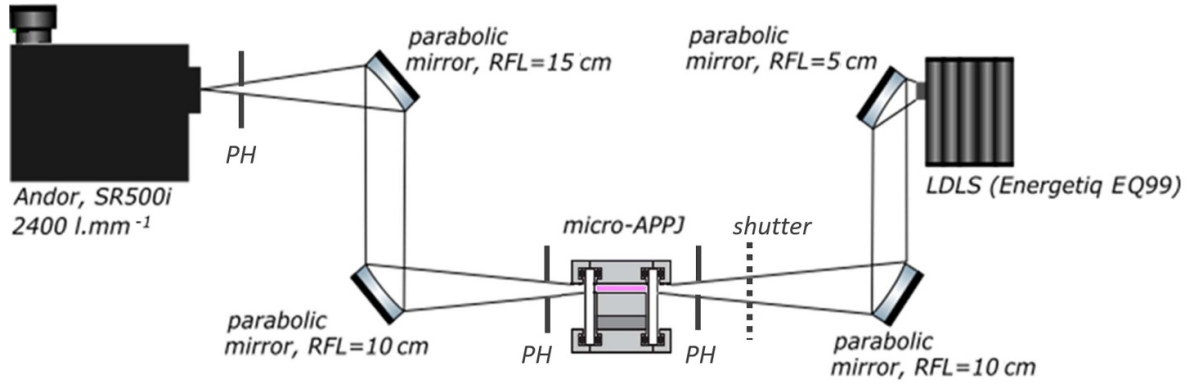


Figure 2. Experimental setup for absorption spectroscopy. RFL: reflective focal length of the mirror, LDLS: laser driven light source, APPJ: atmospheric pressure plasma jet, PH = pinhole.

and light source off (S_B). Each signal is integrated over a time period of 2.5 s after an equally long plasma stabilisation time.

$$T(\lambda) = e^{-A(\lambda)} = \frac{S_T(\lambda)}{S_0(\lambda)} = \frac{S_{P,L} - S_P}{S_L - S_B} \quad (1)$$

$$A(\lambda) = \sigma(\lambda) \times L \times n_{OH}. \quad (2)$$

The observed absorbance is equal to the product of the absorption cross section $\sigma(\lambda)$, the absorption path length L , and the line-of-sight averaged absorber density n_{OH} . A homemade spectrum simulation and fitting programme (see below) is used to find the best least-squared fit of the measured absorbance spectrum, yielding the density and rotational temperature of the lower OH ($X^2\Pi_i, \nu'' = 0$) state. The majority of the population of the electronic ground state lies in the lowest vibrational level, $\nu'' = 0$; no absorption band originating from the $\nu'' = 1$ level was observed. The accuracy of the density measurements depends on the knowledge of the absorption length, here 11 mm with 5% uncertainty. The OH(X) rotational temperature is not necessarily in equilibrium with the gas translational temperature [46].

The absorption spectrum is simulated in the following way. The ro-vibronic energy levels of the upper OH($A^2\Sigma^+, \nu' = 0$) state are calculated according to [51], with Hund's coupling case (b) since $\Lambda = 0$, and the lower OH($X^2\Pi_i, \nu'' = 0$) state, with intermediate case (a) to case (b) coupling. The rotational line strength factors for the 12 electric dipole-allowed branches are calculated using the expressions in [52]. These factors are converted, firstly to relative Einstein coefficients for spontaneous emission, then to absolute ones using the value of 0.698 μs for the radiative lifetime of the lowest rotation level of the OH($A^2\Sigma^+, \nu' = 0$) state [53], and finally to spectrally integrated absorption cross sections for each individual rotational transition. The relative thermal population distribution among the rotation levels of the OH($X^2\Pi_i, \nu'' = 0$) state is calculated according to the rotational Boltzmann factor normalised to the partition sum. For all rotational transitions a common spectral Gaussian line profile is assumed, which represents the resolution of the spectrograph. The intrinsic Doppler

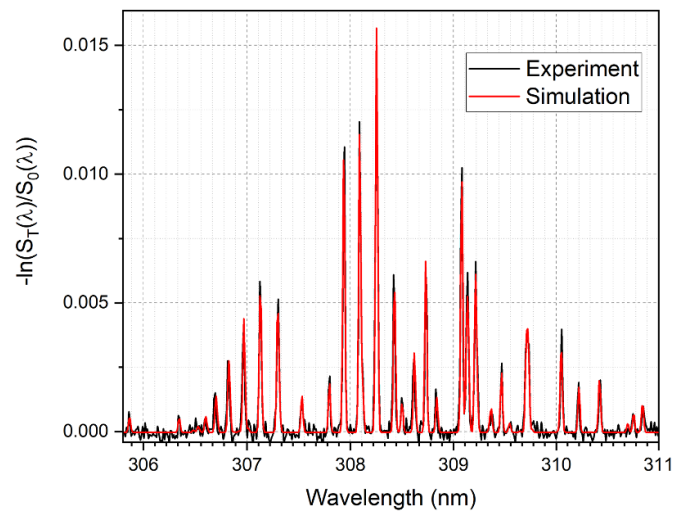


Figure 3. Example of experimental and fitted spectra of the OH ($X^2\Pi_i, \nu'' = 0$) \rightarrow OH ($A^2\Sigma^+, \nu' = 0$) rotational band transition measured by broadband absorption spectroscopy in He + 0.1% O₂ + 0.4% H₂O, for a dissipated power of 15 W cm⁻³. The instrumental width is 0.03 nm.

(0.93 pm at 304 K) and pressure (0.66 pm in helium at 1 atm [54]) broadening are negligible under the given experimental conditions.

Figure 3 shows an example of a measured absorbance spectrum together with the best fit simulation. All measurements were taken at the centre of the reactor, as illustrated by the position of the LDLS beam in figure 1.

2.3. Numerical model for 0D plasma chemistry

In this work, the GlobalKin code is used to describe the RF quasi-homogenous discharge. It is a 0D global plasma-chemical kinetics model which is described in detail in [55]. Briefly, it consists of a reaction chemistry and transport module, a Boltzmann equation solver and an ordinary differential equation solver. In the ordinary differential equation solver, the mass continuity equations for each charged and neutral species are solved as a function of time,

accounting for surface and gas phase production and consumption processes:

$$\frac{dN_i}{dt} = \frac{S}{V} \left(-\frac{D_i N_i \gamma_i}{\gamma_i \Lambda_D + \frac{4D_i}{v_{th,i}}} + \sum_j \frac{D_j N_j \gamma_j f_{ij}}{\gamma_j \Lambda_D + \frac{4D_j}{v_{th,j}}} \right) + S_i. \quad (3)$$

Here, N represents the number density of a species i in the gas phase, $\frac{S}{V}$ is the surface area to volume ratio of the source, Λ_D is the diffusion length, D the diffusion coefficient, γ the surface loss probability, f the return fraction of species from surfaces and S_i represents gas phase production and consumption processes. Here, the diffusion length Λ_D , is calculated as in [43] for a plasma confined in a rectangular chamber, giving a value of 0.0317 cm. Surface losses and gains are calculated using user defined surface loss probabilities as defined in [47]. In addition, the electron energy equation is also solved:

$$\frac{d}{dt} \left(\frac{3}{2} n_e k_B T_e \right) = p_d - \sum_i \frac{3}{2} n_e \nu_{mi} \left(\frac{2m_e}{M_i} \right) k_B (T_e - T_i) + \sum_i n_e k_i N_i \Delta \varepsilon_i. \quad (4)$$

Here, n_e is the electron density, k_B the Boltzmann constant, T_e the electron temperature and p_d represents the plasma power. The second and third terms on the right hand side of the equation represent electron energy changes through elastic and inelastic collisions, respectively. In these terms, ν_{mi} is the electron momentum transfer collision frequency with a species i , m_e the electron mass, M_i the mass of the collision partner, T_i the temperature of the collision partner, k the electron impact rate coefficient and $\Delta \varepsilon_i$ the electron energy changes due to the inelastic collision. A pseudo 1D plug flow model is used to convert the temporally varying densities and temperatures obtained from equations (3) and (4) into spatially varying quantities along the channel of the plasma source using the gas flow velocity. The electron energy distribution function, mean electron energy, electron transport coefficients, and electron impact rate coefficients, are obtained regularly during the simulation, by solving the two-term Boltzmann equation, in this case, every 0.1002 cm. At each point the Boltzmann equation is solved for a range of reduced electric fields and the results tabulated. Values of the electron impact rate coefficients and transport coefficients corresponding to the instantaneous mean electron energy calculated by equation (4) are then used to calculate the relevant source terms in the ordinary differential equations. For all cases, the gas temperature is set to 305 K. Simulations are carried out for plasma electrodes of $3 \times 1 \times 0.1$ cm³ but a plasma volume of $3 \times 1.1 \times 0.1$ cm³ to account for both 0.5 mm gaps between windows and electrodes where the plasma expands. The power density is 15 W cm⁻³ and the flow rate is 5 slm.

The reaction mechanism includes 46 species and 577 reactions and is described in the appendix. It is largely based on the reaction mechanism for He + H₂O mixtures presented in [47]. The reaction set was extended to account for higher O₂ concentrations by adding O-based ions and by refinements to

Table 1. List of the 46 species included in the chemistry set.

	Neutral	Positive	Negative
He	He, He(2 ³ S), He ₂ [*]	He ⁺ , He ₂ ⁺	
O	O, O(¹ D), O(¹ S), O ₂ , O ₂ (a ¹ Δ), O ₂ (b ¹ Σ), O ₃	O ⁺ , O ₂ ⁺ , O ₃ ⁺ , O ₄ ⁺	O ⁻ , O ₂ ⁻ , O ₃ ⁻ , O ₄ ⁻
H	H, H ₂		H ⁻
OH	OH, HO ₂ , H ₂ O, H ₂ O ₂	OH ⁺ , H ₂ O ⁺ (H ₂ O) _{n=0,1} , H ⁺ (H ₂ O) _{n=1-9} , O ₂ ⁺ (H ₂ O)	OH ⁻ , H ₂ O ₂ ⁻ , OH ⁻ (H ₂ O) _{n=1-3}
Other			e

O₃⁺, O₃⁻ and O₄⁻ were added to describe a more complete oxygen-related ion chemistry. Based on the uncertainty analysis of Turner [11, 12], O₂(*v*) and O₃(*v*) are thought to have no significant effect and were not included in the model, helium atomic and molecular metastable states were addressed as single composite states.

some reaction rate coefficients based on the reaction mechanisms for He/O₂ mixtures presented in [9, 11, 12]. The species included in the model are listed in table 1.

3. Results and discussion

In a helium–oxygen–water vapour gas mixture, the density of hydroxyl reaches an approximately constant value within a very short distance in the channel, about 2 mm in our conditions [47]. The results presented hereafter are obtained in the quasi steady-state region of the gas phase, in the middle of the electrodes, 15 mm from the entrance.

3.1. Effects of water vapour and oxygen addition on OH density

To study the effect of water vapour and oxygen on the generation of hydroxyl, various concentrations of water vapour and oxygen are added to the feed gas. The concentration of each added species ranges from 0% to 1%. At higher contents the discharge cannot be sustained.

The density of OH measured by absorption spectroscopy is presented in figure 4 (as squares). The OH density first increases rapidly with humidity content, up to a few tenths of a percent of water vapour, after which the increase is slower. This transition has already been studied [47, 56, 57] and was attributed to the change of electron density and temperature with increasing humidity content, affecting the reaction rate coefficient for OH production. In the absence of O₂, OH is mainly produced by electron impact dissociation of water molecules. However, the water vapour dissociation frequency passes through a maximum, due to competition between an electron temperature increase (increasing the rate coefficient for electron impact dissociation) and electron density decrease (decreasing rate of electron impact dissociation) as the humidity content increases.

Figure 4 also shows the numerical results for similar conditions (as solid lines). The experimental and simulation results

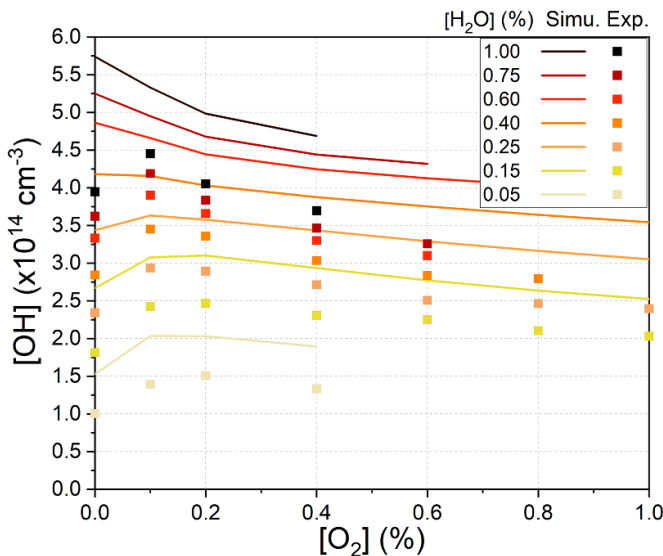


Figure 4. Experimental (squares) and simulation (solid lines) results of OH density in various concentrations of water vapour and oxygen. He flow rate is 5 slm and power density is 15.0 W cm^{-3} .

agree within 50%. The trends are very similar, although the simulation results are somewhat higher by a nearly constant factor. This could be due to an overestimation of the power density ($1\text{--}2 \text{ W cm}^{-3}$, compatible with the uncertainty of the power density measurement indicated in section 2.1) and/or uncertainties in reaction sets and rate coefficients. In addition, in helium-water vapour only, the OH density increase is stronger at high humidity content compared to the experimental results. Despite these discrepancies, the comparison with experiment demonstrates very similar trends and comparable absolute densities, giving confidence in the accuracy of the numerical model.

When molecular oxygen is introduced into the feed gas, it becomes the new dominant source of O-based species, in particular atomic oxygen and ozone. The simulated densities of atomic oxygen are presented in figure 5(a). These are in good agreement with the experimental results presented in [8, 45, 47]. In [8] and [45], nitrogen was also included in the gas mixture at a 4:1 ratio. This comparison may suggest that 0.1% nitrogen has a moderate impact on the atomic oxygen density in dry conditions. However, this comparison should not be considered as a validation of the simulation but simply as a coherent comparison in relatively analogous gases. The density of atomic oxygen increases by one to two orders of magnitude in the presence of 0.1% molecular oxygen compared to He + H₂O only. This is due to the change of the main oxygen-atom production reaction already pointed out in [14]: $\text{OH} + \text{OH} \rightarrow \text{O} + \text{H}_2\text{O}$ in absence of O₂, and electron impact dissociation of O₂ in presence of significant amounts of O₂. On the other hand, as soon as few hundred ppm of water is introduced in a He + O₂ gas admixture, the oxygen-atom loss is mainly due to $\text{OH} + \text{O} \rightarrow \text{O}_2 + \text{H}$, for any concentration of oxygen.

The density of atomic oxygen is predominantly affected by the concentration of molecular oxygen. Nevertheless, it should

be noted that a steep decrease in the O density is observed with increasing water vapour concentration up to about 0.05%, for cases where the O₂ admixture is over 0.025%. Such densities of water vapour could be in the range of impurities or diffusion of ambient humidity in the case of an open plasma source. Over 0.05% water vapour concentration, the O density stabilises progressively and is only slightly affected by further water vapour addition. This observation indicates that the introduction of known amounts of additive species to the feed gas gives better control of ROS production than relying on mixing and diffusion of the effluent into the surrounding environment in the case of open plasma sources [58].

The density of ozone is strongly related to the addition of oxygen to the feed gas (figure 5(b)). It increases by three orders of magnitude with addition of 0.1% O₂. At very low water vapour concentrations, ozone also shows a sharp decrease with water vapour addition, similar to oxygen atoms but not quite as pronounced. Over 0.05% H₂O, the ozone density is only weakly affected by increasing humidity content.

Overall, the simulation results suggest that OH, O and O₃ can be controlled quite independently by varying both water and oxygen concentrations in the feed gas over the range 0%–1% for H₂O and 0.05%–1% for O₂. The OH density depends almost entirely on the water vapour content, while the O and O₃ densities are significantly affected by presence of water vapour, but this effect is relatively independent of the concentration of water vapour for values above 0.05%. Conversely, the O and O₃ densities are more strongly affected by varying the O₂ content. More precisely, the O and O₃ densities drop by approximately an order of magnitude following the addition of up to 0.05% water vapour to a He + O₂ feed gas. If high densities of O and O₃ are required without OH species, then dry conditions appear to be better.

3.2. Analysis of pathways and reaction rates at low water vapour concentration

A detailed analysis of the hydroxyl reaction pathways in the presence of 0.025% water vapour and various concentrations of oxygen is drawn from the chemical kinetics simulation. The dominant reactions for production and consumption of OH, with and without 0.1% O₂, are presented in tables 2 and 3. The analysis is performed at 15 mm into the plasma channel, corresponding to the measurement position. Table 6 presents the corresponding net production rates of the major species as defined in the introduction.

In the absence of molecular oxygen, electron impact reactions generate almost 62% of the hydroxyl radicals. 54% of the OH molecules are produced by dissociation of water molecules by electron impact, and 74% are lost by the recombination of two OH molecules to produce hydrogen peroxide (R(10)) or water plus atomic oxygen (R(11)). The other significant reaction for production of hydroxyl involves the H₂O⁺ ion, responsible for about 30% of OH production. H₂O⁺ is almost entirely produced by two- and three-body Penning ionisation reactions of He(2³S) with water ((He) + He(2³S) + H₂O → (He) + He + H₂O⁺ + e). At low humidity content, the density of secondary species, such

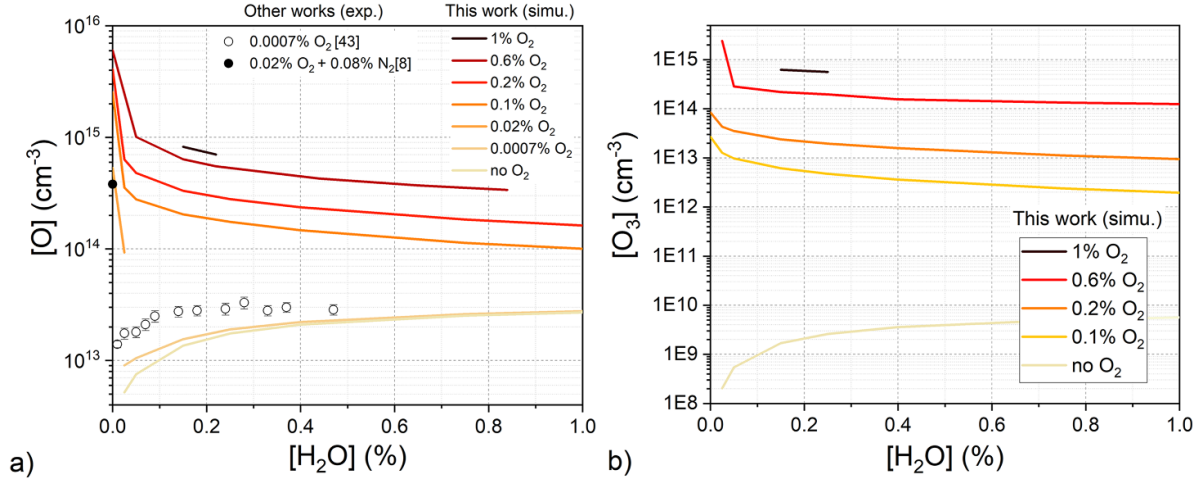


Figure 5. (a) Simulated and measured atomic oxygen densities using various concentrations of water vapour (0.01%–1%) and molecular oxygen (0%–1%). The impurity level of oxygen in the bottle is close to 7 ppm (0.0007%) according to manufacturer specifications. Simulations are only carried out for cases where the level of admixture is low enough to enable plasma ignition. Experimental measurements from [47] are obtained in very similar conditions except at a distance of 1.2 cm from the gas inlet instead of 1.5 cm. Experimental measurements from [8] are obtained in helium flux 10 slm, N₂/O₂ (4:1) admixture 0.1%, and similar driving voltage characteristics (voltage of 234 V). (b) Simulated ozone densities under similar conditions as in (a).

Table 2. Dominant reactions for production of OH in He + 0.025% H₂O (+0.1% O₂) and associated percentage of production and reaction rates (the symbol ‘*v*’ corresponds to the reaction rate in cm⁻³ s⁻¹).

#	Production reactions	He + 0.025% H ₂ O		He + 0.025% H ₂ O + 0.1% O ₂	
		Production of OH (%)	<i>v</i> (cm ⁻³ s ⁻¹)	Production of OH (%)	<i>v</i> (cm ⁻³ s ⁻¹)
R(1)	e + H ₂ O → OH + H + e	40.2	6.36 × 10 ¹⁶	2.4	6.1 × 10 ¹⁶
R(2)	H ₂ O ⁺ + H ₂ O → OH + H ₃ O ⁺	30.1	4.76 × 10 ¹⁶	0.7	1.8 × 10 ¹⁶
R(3)	e + H ₂ O → OH + H ⁻	14	2.21 × 10 ¹⁶	0.8	1.9 × 10 ¹⁶
R(4)	e + H ₂ O ₂ → 2OH + e	7.5	1.19 × 10 ¹⁶	0.8	2.1 × 10 ¹⁶
R(5)	He + H + HO ₂ → He + 2OH	2.7	4.31 × 10 ¹⁵	22.8	5.76 × 10 ¹⁷
R(6)	H ₂ O + O(¹ D) → 2OH	2.7	4.21 × 10 ¹⁵	42.3	1.07 × 10 ¹⁸
R(7)	OH ⁺ + H ₂ O → H ₂ O ⁺ + OH	2.3	3.65 × 10 ¹⁵	Negligible	Negligible
R(8)	O + HO ₂ → OH + O ₂	Negligible	Negligible	21.5	5.44 × 10 ¹⁷
R(9)	H + O ₃ → OH + O ₂	Negligible	Negligible	2.2	5.61 × 10 ¹⁶
	Total from selected reactions	99.5	1.57 × 10¹⁷	97.6	2.41 × 10¹⁸
	Total from all reactions	100	1.58 × 10¹⁷	100	2.53 × 10¹⁸

Table 3. Dominant reactions for consumption of OH in He + 0.025% H₂O (+0.1% O₂) and associated percentage of consumption and reaction rates.

#	Consumption reactions	He + 0.025% H ₂ O		He + 0.025% H ₂ O + 0.1% O ₂	
		Consumption of OH (%)	<i>v</i> (cm ⁻³ s ⁻¹)	Consumption of OH (%)	<i>v</i> (cm ⁻³ s ⁻¹)
R(10)	He + 2OH → He + H ₂ O ₂	53.0	8.28 × 10 ¹⁶	6.3	4.9 × 10 ¹⁷
R(11)	2OH → O + H ₂ O	21.2	3.31 × 10 ¹⁶	2.5	6.34 × 10 ¹⁶
R(12)	He + H + OH → He + H ₂ O	6.3	9.9 × 10 ¹⁵	1.0	2.58 × 10 ¹⁶
R(13)	OH + O → O ₂ + H	12.2	1.9 × 10 ¹⁶	71.9	1.82 × 10 ¹⁸
R(14)	OH + H ₂ O ₂ → HO ₂ + H ₂ O	4.3	4.5 × 10 ¹⁶	0.8	2.06 × 10 ¹⁶
R(15)	OH + HO ₂ → O ₂ + H ₂ O	2.9	6.7 × 10 ¹⁶	17.4	4.4 × 10 ¹⁷
	Total from selected reactions	100	1.56 × 10¹⁷	99.8	2.53 × 10¹⁸
	Total from all reactions	100	1.56 × 10¹⁷	100	2.53 × 10¹⁸

Table 4. Dominant reactions for production of OH in He + 0.75% H₂O (+0.1% O₂) and associated percentage of production and reaction rates (the symbol ‘ ν ’ corresponds to the reaction rate in cm⁻³ s⁻¹).

#	Production reactions	He + 0.75% H ₂ O		He + 0.75% H ₂ O + 0.1% O ₂	
		Production of OH (%)	ν (cm ⁻³ s ⁻¹)	Production of OH (%)	ν (cm ⁻³ s ⁻¹)
R(1)	e + H ₂ O → OH + H + e	51.6	2.59 × 10 ¹⁸	30.7	2.26 × 10 ¹⁸
R(2)	H ₂ O ⁺ + H ₂ O → OH + H ₃ O ⁺	9.2	4.62 × 10 ¹⁷	5.3	3.94 × 10 ¹⁷
R(3)	e + H ₂ O → OH + H ⁻	8.1	4.08 × 10 ¹⁷	4.9	3.58 × 10 ¹⁷
R(4)	e + H ₂ O ₂ → 2OH + e	2.2	1.10 × 10 ¹⁷	1.4	9.3 × 10 ¹⁶
R(5)	He + H + HO ₂ → He + 2OH	22.4	1.13 × 10 ¹⁸	23.7	1.75 × 10 ¹⁸
R(6)	H ₂ O + O(¹ D) → 2OH	3.4	1.71 × 10 ¹⁷	28	2.06 × 10 ¹⁸
R(7)	OH ⁺ + H ₂ O → H ₂ O ⁺ + OH	0.4	2.10 × 10 ¹⁶	Negligible	Negligible
R(16)	H + H ₂ O ₂ → H ₂ O + OH	0.8	4.01 × 10 ¹⁶	Negligible	Negligible
R(8)	O + HO ₂ → OH + O ₂	Negligible	Negligible	3.5	2.55 × 10 ¹⁷
R(9)	H + O ₃ → OH + O ₂	Negligible	Negligible	0.3	2.18 × 10 ¹⁶
	Total from selected reactions	98.1	4.93 × 10¹⁸	97.8	7.19 × 10¹⁸
	Total from all reactions	100	5.03 × 10¹⁸	100	7.37 × 10¹⁸

Table 5. Dominant reactions for consumption of OH in He + 0.75% H₂O(+0.1% O₂) and associated percentage of consumption and reaction rates.

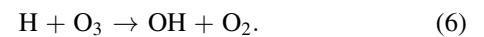
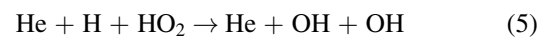
#	Consumption reactions	He + 0.75% H ₂ O		He + 0.75% H ₂ O + 0.1% O ₂	
		Consumption of OH (%)	ν (cm ⁻³ s ⁻¹)	Consumption of OH (%)	ν (cm ⁻³ s ⁻¹)
R(10)	He + 2OH → He + H ₂ O ₂	39.4	1.98 × 10 ¹⁸	23.8	1.76 × 10 ¹⁸
R(11)	2OH → O + H ₂ O	15.7	7.91 × 10 ¹⁷	9.5	7.03 × 10 ¹⁷
R(12)	He + H + OH → He + H ₂ O	13.5	6.80 × 10 ¹⁷	2.4	1.76 × 10 ¹⁷
R(13)	OH + O → O ₂ + H	9.1	4.58 × 10 ¹⁷	26.2	1.94 × 10 ¹⁸
R(14)	OH + H ₂ O ₂ → HO ₂ + H ₂ O	14	7.03 × 10 ¹⁷	8.8	6.49 × 10 ¹⁷
R(15)	OH + HO ₂ → O ₂ + H ₂ O	8.1	4.06 × 10 ¹⁷	29.2	2.15 × 10 ¹⁸
	Total from selected reactions	99.8	5.02 × 10¹⁸	99.9	7.38 × 10¹⁸
	Total from all reactions	100	5.03 × 10¹⁸	100	7.38 × 10¹⁸

as HO₂, is low and the contribution of these species remains small. In particular, HO₂ contributes to only 3% of hydroxyl production and loss. These results are similar to those detailed in [47].

As soon as some oxygen is added to the mixture, the pathways for OH generation change dramatically, even though the resulting OH density remains little changed (see figure 6). The addition of 0.1% O₂ increases the density of atomic oxygen by more than one order of magnitude (figure 5(a)). Consequently, the reaction rates of O-induced reactions are strongly enhanced: the reaction rate of reaction R(6): H₂O + O(¹D) → 2 OH, increases by more than two orders of magnitude, becoming the dominant production reaction of hydroxyl. Loss mechanisms are also modified. Reaction R(13), OH + O → O₂ + H, involving O is greatly enhanced and becomes responsible for 72% of hydroxyl losses. Thus, atomic oxygen is responsible for most of the production as well as the loss of hydroxyl molecules. The calculation of the net production rate of OH by processes involving atomic oxygen, i.e. production reactions R(6) and R(8) minus consumption reaction R(13) (see table 6), shows the net effect O has on the OH density. It reveals that it actually only makes a small alteration to the density of OH at 0.025% H₂O and

0.1% O₂. More precisely, R(6,8,13) have an effective rate of -2.08×10^{17} cm⁻³ s⁻¹ which is -8% of the total production rate of 2.53×10^{18} cm⁻³ s⁻¹. Though dramatically impacting the pathways for OH formation, the O and O(¹D) production and consumption contributions nearly cancel out, leading to a small effective (and negative) contribution to the OH density. This observation remains valid for higher added O₂ concentrations, explaining the nearly constant OH density with O₂ addition (presented in figure 4) for a given low humidity content.

Further analysis of the reaction pathways for OH formation reveals that molecular oxygen has an indirect impact on the OH density. Apart from the O/O(¹D) reactions, the other main production reactions are through the seemingly minor reactions R(5) and R(9):



The density of atomic hydrogen is very similar with and without oxygen admixture, while the densities of HO₂ and O₃

Table 6. Net production rates for OH by major species or groups of species under conditions of low (0.025%) and high (0.75%) water content. The percentage represents the ratio of the net reaction rate of the species to the total production rate of OH.

	He + 0.025% H ₂ O	He + 0.025% H ₂ O + 0.1% O ₂	He + 0.75% H ₂ O	He + 0.75% H ₂ O + 0.1% O ₂
Ratio [O ₂]/[H ₂ O]	0	4	0	0.1
Total production rate of reactions R(1) to R(9) (cm ⁻³ s ⁻¹)	1.58 × 10¹⁷	2.53 × 10¹⁸	5.03 × 10¹⁸	7.37 × 10¹⁸
Electron impact, R(1) + R(3) + R(4)	9.75 × 10¹⁶ (62%)	1.01 × 10¹⁷ (4%)	3.11 × 10¹⁸ (62%)	2.71 × 10¹⁸ (37%)
H ₂ O ⁺ , R(2)	4.76 × 10¹⁶ (30%)	1.81 × 10¹⁶ (<1%)	4.62 × 10¹⁷ (9%)	3.94 × 10¹⁷ (5%)
O + O(1D), R(6) + R(8)—R(13)	-1.49 × 10¹⁶ (-9%)	-2.08 × 10¹⁷ (-8%)	-2.87 × 10¹⁷ (-6%)	3.83 × 10¹⁷ (5%)
HO ₂ , R(5) + R(8)—R(15)	-1.7 × 10¹⁴ (<1%)	6.8 × 10¹⁷ (27%)	7.23 × 10¹⁷ (14%)	-1.50 × 10¹⁷ (-2%)
O ₃ , R(9)	(<1%)	5.61 × 10¹⁶ (2%)	(<1%)	2.18 × 10¹⁶ (<1%)

increase by one to three orders of magnitude with the addition of oxygen. The strong enhancement of HO₂ density (from about 8×10^{11} to 5×10^{13} cm⁻³) comes from the increased rate of $\text{He} + \text{H} + \text{O}_2 \rightarrow \text{He} + \text{HO}_2$ with addition of 0.1% molecular oxygen. This reaction is more efficient than the additional loss reaction: $\text{HO}_2 + \text{O} \rightarrow \text{OH} + \text{O}_2$. The effective contribution of HO₂-induced reactions (R5,8,15) represents 27% of OH production at low water content (0.025% H₂O) and 0.1% O₂ (see table 6). The role of reaction (5) on the OH kinetics was also identified in a recent study of a He + O₂ + H₂O pulsed plasma jet at 1 kHz and 10 kV [59].

For relatively low concentrations of oxygen, the role played by ozone is minor. However, it grows with the increasing oxygen addition since ozone is dominantly produced by: $\text{He} + \text{O}_2 + \text{O} \rightarrow \text{He} + \text{O}_3$. Subsequently, through reaction (6), it produces non-negligible amounts of OH radicals, representing 2% of the OH formation at 0.1% O₂ (effective rate 5.6×10^{16} cm⁻³ s⁻¹) and about 10% at 0.5% O₂ (reaction rates at 0.5% O₂ are not detailed here).

3.3. Analysis of pathways and reaction rates at high water vapour concentration (0.75% H₂O)

Now let us consider a similar analysis of the hydroxyl reaction pathways in the presence of 0.75% water vapour and various concentrations of oxygen. The dominant reactions for the production and consumption of OH with and without 0.1% O₂ are presented in tables 4 and 5. The corresponding net production rates of the major species can be found in table 6.

In the absence of molecular oxygen, at the highest water concentration studied (0.75% H₂O), the reaction rates of all OH related reactions increase significantly and the relative importance of the different production or loss reactions of OH change compared to low humidity conditions (0.025% H₂O). The density of most H-containing species increases dramatically, in particular for the secondary species H₂O₂ and HO₂. The H density increases to a lesser extent, while OH and O show a similar increase. Conversely, the positive ions

H₂O⁺ and OH⁺ decrease by up to an order of magnitude, due to a decrease in electron density, affecting the density of their precursor species, He(2³S) which are created through electron impact reactions.

Three main points can be made. The dissociation of H₂O by electron impact remains the dominant reaction for OH production. But as mentioned above, due to the decrease in electron density as the water vapour concentration increases, OH production is reduced above a certain water vapour content. Also, with the larger increase of secondary species densities compared to other species, reactions R(5, 8, 14, 15) are promoted. In particular, reaction (5) now accounts for more than a fifth of the production of OH, against 2.7% with only 0.025% H₂O. Among the loss mechanisms of OH, reactions involving secondary species (H₂O₂, HO₂) also play a more significant role. The recombination of two OH molecules now only accounts for half of the losses, against three-quarters at 0.025% H₂O. The effective reaction rate of HO₂ has an increased role in OH production; it goes from having a negligible contribution at low water vapour content to making +14% of OH formation (see table 6). It is noteworthy that reaction R(2) has a decreased relative contribution due to the significant decrease in H₂O⁺ ion density; the ratio $[\text{H}_2\text{O}^+]/[\text{H}_2\text{O}]$ drops by two orders of magnitude compared to its value at 0.025% H₂O.

In the presence of 0.1% molecular oxygen and 0.75% water vapour, the plasma chemistry does not tend towards a pure water vapour chemistry, in contrast to the low humidity case (0.025%). The effect of high amounts of both water vapour and oxygen leads to the development of complex pathways for OH formation. Thus, the chemistry exhibits strong characteristics of both water vapour and oxygen-induced pathways. In this way, OH is produced approximately equally by electron-impact dissociation of water and by the O(1D)-induced reaction R(6). The following comments compare a gas mixture with 0.1% O₂ at low humidity (He + 0.025% H₂O + 0.1% O₂) to a high humidity case (He + 0.75% H₂O + 0.1% O₂). The latter reaction R(6), largely benefits from the increase of water density: the reaction rate of R(6) increases by 193%

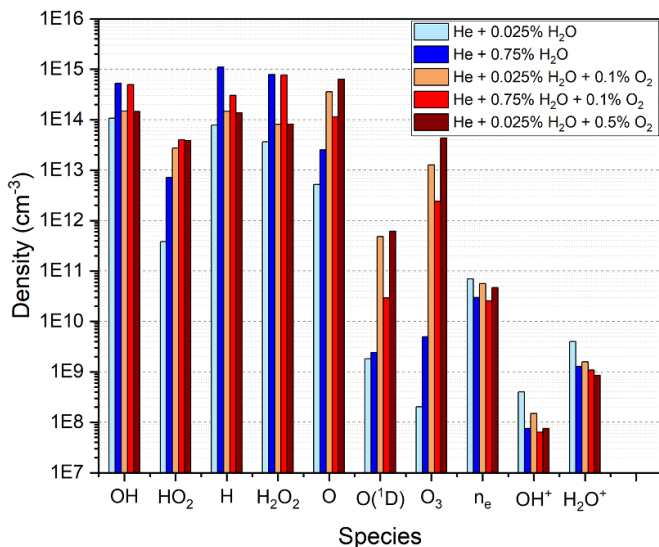


Figure 6. Density of some major O- and H-species for different conditions. Addition of large amounts of O₂ only significantly benefits to the production of O₃.

from low to high humidity, while the reaction rate of R(13) remains almost unchanged. This means that large concentrations of water vapour are necessary for the net contribution of atomic oxygen R(6, 8, 13) to increase the production of OH. Nevertheless, O and O(¹D) contributions remain low at high humidity, about +5% of OH production rate (3.83×10^{17} out of $7.37 \times 10^{18} \text{ cm}^{-3} \text{ s}^{-1}$). In addition, the secondary species HO₂ which accounted for a quarter of OH formation at low humidity content has a negligible impact on OH formation (−2%) at high humidity. This is due to the strong drop of O density with higher water concentration, affecting the R(8) reaction rate.

These complex interactions show that even with only two additives, the chemistry cannot be easily tailored, and a detailed analysis of reaction rates must be undertaken for that purpose.

Focusing on O and O(¹D), their generation mechanisms are very different, and change according to the gas mixture.

If water vapour is the only admixture, both the production and loss mechanisms of ground-state atomic oxygen depend dominantly on OH and do not change significantly with increasing water content. Consequently, the density of O increases almost proportionally with OH (+490% from 0.025% to 0.75% added water vapour) and the density of O may be inferred from the density of OH if it is known in one condition. The generation mechanisms of O(¹D) are different, but again they do not change significantly with increasing water content. O(¹D) production depends on low density secondary species (mostly O₂, O₂^{*} and O) and a little on water vapour. Therefore, the O(¹D) density does not increase significantly from low to high humidity content.

In the presence of molecular oxygen, in dry conditions, O and O(¹D) are largely produced by dissociation of O₂ by electron impact. O(¹D) mainly decays to O through: O(¹D) + O₂ → O + O₂(b¹Σ_g⁺). The densities of O and O(¹D) increase by

two orders of magnitude compared to the case with water only (figures 5 and 6). O reaches $5 \times 10^{14} \text{ cm}^{-3}$ in He + 0.02% O₂, similar to the experimental value from [8] obtained in helium with 0.1% dry air (see legend of figure 5 for other experimental conditions) and reaches 10^{15} cm^{-3} in He + 0.1% O₂. The loss of O is mainly due to O gas-phase recombination mechanisms. Diffusion to the walls is typically the second most important loss process but it only represents a few percent of the overall losses. However, when some water vapour is introduced, OH and HO₂ become largely responsible for the loss of O. O(¹D) is very efficiently quenched by water to form 2 OH, so that the decay to O becomes less significant. O losses are significantly higher in the presence of water vapour causing the density of O to drop by an order of magnitude from dry to low humidity conditions. As the humidity content increases from 0.05% to 1%, the variations are much smaller and the O density decreases by at most a factor 3.

Finally, figure 6 illustrates the variations of the densities of the major ROS and the electron density for the most representative admixtures. It also includes the densities simulated in He + 0.025% O₂ + 0.5% O₂ in order to accentuate the role of O₂-induced reactions. It highlights that adding small (0.1%) or large (0.5%) concentrations of O₂ does not significantly affect the density of H-species (apart from HO₂). However, large concentrations of O₂ (0.5% O₂) significantly increase the production of O₃. From 0.1% to 0.5% added oxygen, the ozone density rises by a factor 4 ($1-4 \times 10^{13} \text{ cm}^{-3}$).

4. Conclusion

This work presents measurements of the density of OH radicals in a He + O₂ + H₂O RF plasma at atmospheric pressure. The measurements were made using an ultra-sensitive broadband absorption spectroscopy setup. The results are mostly in agreement with previous numerical analyses [14, 41]. The plasma chemistry is also analysed using OD plasma-chemical kinetics simulations. The simulated and experimental results are compared in order to understand the kinetics of the major ROS, in particular OH, O, O(¹D) and HO₂, over a wide range of water and oxygen concentrations. The analysis of reaction rates enabled the identification of the net contributions of each species to the generation or loss of OH and O.

In He + H₂O, OH is created principally by electron impact dissociation of water vapour, and lost by three-body recombination of two OH molecules to form H₂O₂. The density of OH increases from 1.0×10^{14} to $4.0 \times 10^{14} \text{ cm}^{-3}$ for H₂O admixtures from 0.05% to 1%. The density of atomic oxygen is of the order of $1 \times 10^{13} \text{ cm}^{-3}$. When water vapour is the only molecular admixture in the gas, the density of O increases nearly proportionally with OH over the studied range and may be inferred from the density of OH, and inversely. The experimental measurements and simulation results of OH and O densities are in good agreement. The discrepancies in OH densities between the two approaches are within 50%.

In the presence of molecular oxygen, the OH formation pathways are strongly modified. Nevertheless, the OH density

is not significantly affected because the dominant O and O(¹D)-induced production and consumption contributions to OH formation nearly cancel out. However, the introduction of around 0.1% molecular oxygen increases the density of O-species (O, O(¹D), O₃) by several orders of magnitude. This also favours HO₂ production, through $H + O_2 + He \rightarrow HO_2 + He$, which plays a significant role in OH formation at low water content. The density of the other H-species such as OH are not strongly affected by the addition of molecular oxygen as long as the total amount of impurities remains below 1%. The introduction of larger concentrations of oxygen only has a strong impact on the ozone density.

Therefore, it can be concluded that OH, O and O₃ can be tuned relatively independently by varying the concentration of water and oxygen in the feed gas. The OH density is not strongly affected by the oxygen content, but is instead determined by the water vapour content. The O and O₃ densities, on the other hand, are strongly affected by O₂ addition whether or not water vapour is added, but the effect is relatively independent of the concentration of water vapour as long as it is above 0.05%, with their densities then mainly controlled by the O₂

content. Below 0.05% water vapour, the O and O₃ densities are strongly decreased by water addition, and independent control of OH, O and O₃ is not possible. A perfectly dry environment is preferable if higher amounts of O and O₃ are required without OH species.

Data availability statement

The data that support the findings of this study are openly available at the following URL/DOI: <https://doi.org/10.15124/6ebd6e18-17e5-4cf1-80cc-04379f58a1e7>.

Acknowledgment

This work was supported by the EP/S026584/1 and EP/K018388/1 research programs. The authors would like to thank Professor Mark Kushner for providing the GlobalKin code used in this work, and for continued useful discussions. The authors are also thankful to Dr Helen Davies for advising with the simulations.

Appendix

No.	Reaction	Rate Coefficient ^{a,b}	Ref.
Elastic scattering and momentum transfer			
1	$e + \text{He} \rightarrow \text{He} + e$	$f(\epsilon)$	[60, 61]
2	$e + \text{H}_2\text{O} \rightarrow \text{H}_2\text{O} + e$	$f(\epsilon)$	[62, 63]
3	$e + \text{O}_2 \rightarrow \text{O}_2 + e$	$f(\epsilon)$	[64]
Electron impact excitation and ionisation			
4	$e + \text{He} \rightarrow e + \text{He}(2^3\text{S})$	$f(\epsilon)$	[60, 61]
5	$e + \text{He} \rightarrow e + \text{He}(2^3\text{S})$	$f(\epsilon)$	[60, 61]
6	$e + \text{He} \rightarrow \text{He}^+ + e + e$	$f(\epsilon)$	[60, 61]
7	$e + \text{He}(2^3\text{S}) \rightarrow \text{He}^+ + 2e$	$f(\epsilon)$	[65] ^c
8	$e + \text{He}_2^* \rightarrow \text{He}_2^+ + 2e$	$2.06 \times 10^{-13} e^{-4.28/T_e}$	[66] ^d
9	$e + \text{OH} \rightarrow \text{OH}^+ + 2e$	$f(\epsilon)$	[67]
10	$e + \text{H}_2\text{O} \rightarrow \text{H}_2\text{O} + e$	$f(\epsilon)$	[62] ^e
11	$e + \text{H}_2\text{O} \rightarrow \text{H}_2\text{O} + e$	$f(\epsilon)$	[62] ^e
12	$e + \text{H}_2\text{O} \rightarrow \text{H}_2\text{O} + e$	$f(\epsilon)$	[62] ^e
13	$e + \text{H}_2\text{O} \rightarrow \text{H}_2\text{O}^+ + 2e$	$f(\epsilon)$	[62]
14	$e + \text{O} \rightarrow \text{O}(^1\text{D}) + e$	$f(\epsilon)$	[68]
15	$e + \text{O} \rightarrow \text{O}(^1\text{S}) + e$	$f(\epsilon)$	[68]
16	$e + \text{O} \rightarrow \text{O}^+ + 2e$	$f(\epsilon)$	[68]
17	$e + \text{O}(^1\text{D}) \rightarrow \text{O}^+ + 2e$	$f(\epsilon)$	[65] ^c
18	$e + \text{O}(^1\text{S}) \rightarrow \text{O}^+ + 2e$	$f(\epsilon)$	[69] ^c
19	$e + \text{O}_2 \rightarrow \text{O}_2 + e$	$f(\epsilon)$	[64] ^f
20	$e + \text{O}_2 \rightarrow \text{O}_2 + e$	$f(\epsilon)$	[64] ^e
21	$e + \text{O}_2 \rightarrow \text{O}_2 + e$	$f(\epsilon)$	[64] ^e
22	$e + \text{O}_2 \rightarrow \text{O}_2 + e$	$f(\epsilon)$	[64] ^e
23	$e + \text{O}_2 \rightarrow \text{O}_2 + e$	$f(\epsilon)$	[64] ^e
24	$e + \text{O}_2 \rightarrow \text{O}_2 + e$	$f(\epsilon)$	[64] ^e
25	$e + \text{O}_2 \rightarrow \text{O}_2 + e$	$f(\epsilon)$	[64] ^e
26	$e + \text{O}_2 \rightarrow \text{O}_2(a^1\Delta) + e$	$f(\epsilon)$	[64]
27	$e + \text{O}_2 \rightarrow \text{O}_2(b^1\Sigma) + e$	$f(\epsilon)$	[64]
28	$e + \text{O}_2 \rightarrow \text{O}_2(b^1\Sigma) + e$	$f(\epsilon)$	[64]
29	$e + \text{O}_2 \rightarrow \text{O}_2^+ + 2e$	$f(\epsilon)$	[64]
30	$e + \text{O}_2(a^1\Delta) \rightarrow \text{O}_2(a^1\Delta) + e$	$f(\epsilon)$	As reaction 19 ^g
31	$e + \text{O}_2(a^1\Delta) \rightarrow \text{O}_2(a^1\Delta) + e$	$f(\epsilon)$	As reaction 20 ^g
g32	$e + \text{O}_2(a^1\Delta) \rightarrow \text{O}_2(a^1\Delta) + e$	$f(\epsilon)$	As reaction 21 ^g
33	$e + \text{O}_2(a^1\Delta) \rightarrow \text{O}_2(a^1\Delta) + e$	$f(\epsilon)$	As reaction 22 ^g
34	$e + \text{O}_2(a^1\Delta) \rightarrow \text{O}_2(a^1\Delta) + e$	$f(\epsilon)$	As reaction 23 ^g
35	$e + \text{O}_2(a^1\Delta) \rightarrow \text{O}_2(a^1\Delta) + e$	$f(\epsilon)$	As reaction 24 ^g
36	$e + \text{O}_2(a^1\Delta) \rightarrow \text{O}_2(a^1\Delta) + e$	$f(\epsilon)$	As reaction 25 ^g
37	$e + \text{O}_2(a^1\Delta) \rightarrow \text{O}_2(b^1\Sigma) + e$	$f(\epsilon)$	[70] ^h
38	$e + \text{O}_2(a^1\Delta) \rightarrow \text{O}_2(b^1\Sigma) + e$	$f(\epsilon)$	As reaction 28 ^g
39	$e + \text{O}_2(a^1\Delta) \rightarrow \text{O}_2^+ + 2e$	$f(\epsilon)$	As reaction 29 ^g
40	$e + \text{O}_2(b^1\Sigma) \rightarrow \text{O}_2(b^1\Sigma) + e$	$f(\epsilon)$	As reaction 19 ^g
41	$e + \text{O}_2(b^1\Sigma) \rightarrow \text{O}_2(b^1\Sigma) + e$	$f(\epsilon)$	As reaction 20 ^g
42	$e + \text{O}_2(b^1\Sigma) \rightarrow \text{O}_2(b^1\Sigma) + e$	$f(\epsilon)$	As reaction 21 ^g
43	$e + \text{O}_2(b^1\Sigma) \rightarrow \text{O}_2(b^1\Sigma) + e$	$f(\epsilon)$	As reaction 22 ^g
44	$e + \text{O}_2(b^1\Sigma) \rightarrow \text{O}_2(b^1\Sigma) + e$	$f(\epsilon)$	As reaction 23 ^g
45	$e + \text{O}_2(b^1\Sigma) \rightarrow \text{O}_2(b^1\Sigma) + e$	$f(\epsilon)$	As reaction 24 ^g
46	$e + \text{O}_2(b^1\Sigma) \rightarrow \text{O}_2(b^1\Sigma) + e$	$f(\epsilon)$	As reaction 25 ^g
47	$e + \text{O}_2(b^1\Sigma) \rightarrow \text{O}_2(b^1\Sigma) + e$	$f(\epsilon)$	As reaction 28 ^g
48	$e + \text{O}_2(b^1\Sigma) \rightarrow \text{O}_2^+ + 2e$	$f(\epsilon)$	As reaction 29 ^g
49	$e + \text{O}_3 \rightarrow \text{O}_3^+ + 2e$	$5.96 \times 10^{-15} T_e^{0.978} e^{-12.55/T_e}$	[11, 71, 72]

(Continued.)

No.	Reaction	Rate Coefficient ^{a,b}	Ref.
Super-elastic collisions			
50	$e + \text{He}(2^3\text{S}) \rightarrow \text{He} + e$	$f(\epsilon)$	[60, 61] ⁱ
51	$e + \text{O}(^1\text{D}) \rightarrow \text{O} + e$	$f(\epsilon)$	[68] ⁱ
52	$e + \text{O}(^1\text{S}) \rightarrow \text{O} + e$	$f(\epsilon)$	[68] ⁱ
53	$e + \text{O}_2(\text{a}^1\Delta) \rightarrow \text{O}_2 + e$	$f(\epsilon)$	[64] ⁱ
54	$e + \text{O}_2(\text{b}^1\Sigma) \rightarrow \text{O}_2 + e$	$f(\epsilon)$	[64] ⁱ
55	$e + \text{O}_2(\text{b}^1\Sigma) \rightarrow \text{O}_2(\text{a}^1\Delta) + e$	$f(\epsilon)$	As reaction 37 ⁱ
Electron impact dissociation			
56	$e + \text{He}_2^* \rightarrow 2 \text{He} + e$	3.80×10^{-15}	[73]
57	$e + \text{H}_2\text{O} \rightarrow \text{O}(^1\text{S}) + 2 \text{H} + e$	$f(\epsilon)$	[62, 74]
58	$e + \text{H}_2\text{O} \rightarrow \text{H} + \text{OH} + e$	$f(\epsilon)$	[62, 75]
59	$e + \text{H}_2\text{O} \rightarrow \text{H} + \text{OH} + e$	$f(\epsilon)$	[62]
60	$e + \text{H}_2\text{O} \rightarrow \text{H}_2 + \text{O}(^1\text{D}) + e$	$2.416 \times 10^{-14} T_e^{-0.062} e^{-22.4/T_e}$	[76] ^j
61	$e + \text{H}_2 \rightarrow 2 \text{H} + e$	$f(\epsilon)$	[77]
62	$e + \text{H}_2 \rightarrow 2 \text{H} + e$	$f(\epsilon)$	[78]
63	$e + \text{OH} \rightarrow \text{O} + \text{H} + e$	$f(\epsilon)$	[79] ^k
64	$e + \text{H}_2\text{O}_2 \rightarrow 2\text{OH} + e$	2.36×10^{-15}	[80] ^l
65	$e + \text{O}_2 \rightarrow 2\text{O} + e$	$f(\epsilon)$	[64]
66	$e + \text{O}_2 \rightarrow \text{O} + \text{O}(^1\text{D}) + e$	$f(\epsilon)$	[64]
67	$e + \text{O}_2 \rightarrow 2\text{O}(^1\text{D}) + e$	$f(\epsilon)$	[64]
68	$e + \text{O}_2(\text{a}^1\Delta) \rightarrow 2\text{O} + e$	$f(\epsilon)$	As reaction 65 ^g
69	$e + \text{O}_2(\text{a}^1\Delta) \rightarrow \text{O} + \text{O}(^1\text{D}) + e$	$f(\epsilon)$	As reaction 66 ^g
70	$e + \text{O}_2(\text{a}^1\Delta) \rightarrow 2\text{O}(^1\text{D}) + e$	$f(\epsilon)$	As reaction 67 ^g
71	$e + \text{O}_2(\text{b}^1\Sigma) \rightarrow 2\text{O} + e$	$f(\epsilon)$	As reaction 65 ^g
72	$e + \text{O}_2(\text{b}^1\Sigma) \rightarrow \text{O} + \text{O}(^1\text{D}) + e$	$f(\epsilon)$	As reaction 66 ^g
73	$e + \text{O}_2(\text{b}^1\Sigma) \rightarrow 2\text{O}(^1\text{D}) + e$	$f(\epsilon)$	As reaction 67 ^g
74	$e + \text{O}_3 \rightarrow \text{O} + \text{O}_2 + e$	$1.70 \times 10^{-14} T_e^{-0.57} e^{-2.48/T_e}$	[11, 81]
75	$e + \text{O}_3 \rightarrow \text{O}(^1\text{D}) + \text{O}_2(\text{a}^1\Sigma) + e$	$3.22 \times 10^{-13} T_e^{-1.18} e^{-9.17/T_e}$	[11, 81]
Dissociative ionisation			
76	$e + \text{H}_2\text{O} \rightarrow \text{OH}^+ + \text{H} + 2e$	$f(\epsilon)$	[62]
77	$e + \text{H}_2\text{O} \rightarrow \text{O}^+ + 2 \text{H} + 2e$	$f(\epsilon)$	[62]
78	$e + \text{O}_2 \rightarrow \text{O} + \text{O}^+ + 2e$	$f(\epsilon)$	[82]
79	$e + \text{O}_2(\text{a}^1\Delta) \rightarrow \text{O} + \text{O}^+ + 2e$	$f(\epsilon)$	As reaction 78 ^g
80	$e + \text{O}_2(\text{b}^1\Sigma) \rightarrow \text{O} + \text{O}^+ + 2e$	$f(\epsilon)$	As reaction 78 ^g
(Dissociative) electron attachment			
81	$e + \text{H}_2\text{O} \rightarrow \text{OH}^- + \text{H}^-$	$f(\epsilon)$	[62, 83]
82	$e + \text{H}_2\text{O} \rightarrow \text{H}_2 + \text{O}^-$	$f(\epsilon)$	[62, 83]
83	$e + \text{H}_2\text{O} \rightarrow \text{OH}^- + \text{H}$	$f(\epsilon)$	[62, 83]
84	$e + \text{H}_2\text{O}_2 \rightarrow \text{H}_2\text{O} + \text{O}^-$	$f(\epsilon)$	[84]
85	$e + \text{H}_2\text{O}_2 \rightarrow \text{OH}^- + \text{OH}^-$	$f(\epsilon)$	[84]
86	$e + \text{O}_2 \rightarrow \text{O} + \text{O}^-$	$f(\epsilon)$	[64]
87	$e + \text{O}_2(\text{a}^1\Delta) \rightarrow \text{O} + \text{O}^-$	$f(\epsilon)$	[85]
88	$e + \text{O}_2(\text{b}^1\Sigma) \rightarrow \text{O} + \text{O}^-$	$f(\epsilon)$	As reaction 87 ^g
89	$e + \text{O}_3 \rightarrow \text{O}_2 + \text{O}^-$	$f(\epsilon)$	[86]
90	$e + \text{O}_3 \rightarrow \text{O}_2^- + \text{O}$	$f(\epsilon)$	[86]

(Continued.)

No.	Reaction	Rate Coefficient ^{a,b}	Ref.
Electron detachment			
91	$e + H^- \rightarrow H + 2e$	$f(\epsilon)$	[87]
92	$e + OH^- \rightarrow OH + 2e$	$f(\epsilon)$	[88]
93	$e + O^- \rightarrow O + 2e$	$f(\epsilon)$	[89]
94	$e + O_2^- \rightarrow O_2 + 2e$	$f(\epsilon)$	[90]
95	$e + O_3^- \rightarrow O_3 + 2e$	$2.12 \times 10^{-14} T_e^{0.51} e^{-5.87/T_e}$	[11, 91]
96	$e + O_3^- \rightarrow O_2 + O + 2e$	$7.12 \times 10^{-14} T_e^{-0.132} e^{-5.94/T_e}$	[11, 91]
97	$e + O_3^- \rightarrow 3O + 2e$	$1.42 \times 10^{-14} T_e^{-0.52} e^{-9.30/T_e}$	[11, 91]
Electron-ion Recombination			
98	$e + He^+ \rightarrow He(2^3S)$	$f(\epsilon)$	[92]
99	$e + He_2^+ \rightarrow He + He(2^3S)$	$9.60 \times 10^{-17} T_e^{-0.5}$	[93]
100	$e + H_2O^+ \rightarrow O + 2H$	$3.05 \times 10^{-13} T_e^{-0.5}$	[94, 95]
101	$e + H_2O^+ \rightarrow O + H_2$	$3.87 \times 10^{-14} T_e^{-0.5}$	[94, 95]
102	$e + H_2O^+ \rightarrow H + OH$	$8.60 \times 10^{-14} T_e^{-0.5}$	[94, 95]
103	$e + H^+(H_2O) \rightarrow H + H_2O$	$7.09 \times 10^{-14} T_e^{-0.5}$	[94, 96, 97]
104	$e + H^+(H_2O) \rightarrow OH + H_2$	$5.37 \times 10^{-14} T_e^{-0.5}$	[94, 96, 97]
105	$e + H^+(H_2O) \rightarrow OH + 2H$	$3.05 \times 10^{-13} T_e^{-0.5}$	[94, 96, 97]
106	$e + O_2^+(H_2O) \rightarrow O_2 + H_2O$	$7.22 \times 10^{-13} T_e^{-0.2}$	[98]
107	$e + H_2O^+(H_2O) \rightarrow H + OH + H_2O$	$9.63 \times 10^{-13} T_e^{-0.2}$	[98] ^m
108	$e + H^+(H_2O)_2 \rightarrow H + 2H_2O$	$1.87 \times 10^{-12} T_e^{-0.08}$	[99]
109	$e + H^+(H_2O)_3 \rightarrow H + 3H_2O$	$2.24 \times 10^{-12} T_e^{-0.08}$	[99]
110	$e + H^+(H_2O)_4 \rightarrow H + 4H_2O$	3.60×10^{-12}	[99]
111	$e + H^+(H_2O)_5 \rightarrow H + 5H_2O$	4.10×10^{-12}	[100]
112	$e + H^+(H_2O)_6 \rightarrow H + 6H_2O$	5.13×10^{-12}	[100]
113	$e + H^+(H_2O)_7 \rightarrow H + 7H_2O$	1.00×10^{-12}	[100]
114	$e + H^+(H_2O)_8 \rightarrow H + 8H_2O$	4.10×10^{-12}	As reaction 111
115	$e + H^+(H_2O)_9 \rightarrow H + 9H_2O$	4.10×10^{-12}	As reaction 111
116	$e + O^+ \rightarrow O(^1D)$	2.70×10^{-19}	[11, 98]
117	$e + O_2^+ \rightarrow 2O$	$3.79 \times 10^{-15} T_e^{-0.7}$	[101]
118	$e + O_2^+ \rightarrow O + O(^1D)$	$8.17 \times 10^{-15} T_e^{-0.7}$	[101]
119	$e + O_2^+ \rightarrow 2O(^1D)$	$5.85 \times 10^{-15} T_e^{-0.7}$	[101]
120	$e + O_3^+ \rightarrow 3O$	$2.07 \times 10^{-13} T_e^{-0.55}$	[11, 102]
121	$e + O_3^+ \rightarrow 2O + O(^1D)$	$6.69 \times 10^{-13} T_e^{-0.55}$	[11, 102]
122	$e + O_3^+ \rightarrow O + 2O(^1D)$	$1.55 \times 10^{-13} T_e^{-0.55}$	[11, 102]
123	$e + O_4^+ \rightarrow O + O(^1D) + O_2$	2.02×10^{-14}	[11, 93, 103]
124	$e + O_4^+ \rightarrow O(^1D) + O(^1S) + O_2$	1.35×10^{-14}	[11, 93, 103]

^a In $m^3 s^{-1}$ and $m^6 s^{-1}$ for two- and three-body processes, respectively.

^b $f(E)$ denotes rate coefficients are calculated by the internal GlobalKin two-term Boltzmann equation solver using cross sections obtained from the indicated literature.

^c Cross sections are calculated from an expression in cited reference.

^d Calculated assuming a Maxwell distribution function and cross sections from the given relevant reference.

^e Vibrational excitation cross section included in cross section set for two-term Boltzmann solver. Vibrational states not simulated self-consistently in reaction kinetics.

^f Rotational excitation cross section included in cross section set for two-term Boltzmann solver. Rotations states not simulated self-consistently in reaction kinetics.

^g Cross section estimated by shifting and scaling the corresponding cross section for the ground state by the excitation threshold of the excited state.

^h Born–Bethe fit to data in the cited reference.

ⁱ Obtained from reverse process by detailed balance.

^j In the reference reaction rates were calculated using Bolsig+ [104] and cross sections obtained from the Morgan database [105] for a He/H₂O plasma.

^k Cross section assumed to be the same as that for CO.

^l Value is approximated in reference based on cross section for electron impact dissociation of O₂.

^m Value is estimated in reference.

No.	Reaction	Rate Coefficient ^a	Ref.
177	$O_4^+ + O_3^- + He \rightarrow 2O_2 + O_3 + He$	$2.00 \times 10^{-37} (T_g/300)^{-2.5}$	[106] ^b
178	$O_4^+ + O_4^- + He \rightarrow 4O_2 + He$	$2.00 \times 10^{-37} (T_g/300)^{-2.5}$	[106] ^b
179	$O_4^+ + H^- + He \rightarrow 2O_2 + H + He$	$2.00 \times 10^{-37} (T_g/300)^{-2.5}$	[106] ^b
180	$O_4^+ + OH^- + He \rightarrow 2O_2 + OH + He$	$2.00 \times 10^{-37} (T_g/300)^{-2.5}$	[106] ^b
181	$O_4^+ + H_2O_2^- + He \rightarrow 2O_2 + H_2O_2 + He$	$2.00 \times 10^{-37} (T_g/300)^{-2.5}$	[106] ^b
182	$O_4^+ + OH^-(H_2O) + He \rightarrow 2O_2 + H_2O + OH + He$	$2.00 \times 10^{-37} (T_g/300)^{-2.5}$	[106] ^b
183	$O_4^+ + OH^-(H_2O)_2 + He \rightarrow 2O_2 + 2H_2O + OH + He$	$2.00 \times 10^{-37} (T_g/300)^{-2.5}$	[106] ^b
184	$O_4^+ + OH^-(H_2O)_3 + He \rightarrow 2O_2 + 3H_2O + OH + He$	$2.00 \times 10^{-37} (T_g/300)^{-2.5}$	[106] ^b
185	$OH^+ + O^- + He \rightarrow OH + O + He$	$2.00 \times 10^{-37} (T_g/300)^{-2.5}$	[106] ^b
186	$OH^+ + O_2^- + He \rightarrow OH + O_2 + He$	$2.00 \times 10^{-37} (T_g/300)^{-2.5}$	[106] ^b
187	$OH^+ + O_3^- + He \rightarrow OH + O_3 + He$	$2.00 \times 10^{-37} (T_g/300)^{-2.5}$	[106] ^b
188	$OH^+ + O_4^- + He \rightarrow OH + 2O_2 + He$	$2.00 \times 10^{-37} (T_g/300)^{-2.5}$	[106] ^b
189	$OH^+ + H^- + He \rightarrow OH + H + He$	$2.00 \times 10^{-37} (T_g/300)^{-2.5}$	[106] ^b
190	$OH^+ + OH^- + He \rightarrow 2OH + He$	$2.00 \times 10^{-37} (T_g/300)^{-2.5}$	[106] ^b
191	$OH^+ + H_2O_2^- + He \rightarrow OH + H_2O_2 + He$	$2.00 \times 10^{-37} (T_g/300)^{-2.5}$	[106] ^b
192	$OH^+ + OH^-(H_2O) + He \rightarrow 2OH + H_2O + He$	$2.00 \times 10^{-37} (T_g/300)^{-2.5}$	[106] ^b
193	$OH^+ + OH^-(H_2O)_2 + He \rightarrow 2OH + 2H_2O + He$	$2.00 \times 10^{-37} (T_g/300)^{-2.5}$	[106] ^b
194	$OH^+ + OH^-(H_2O)_3 + He \rightarrow 2OH + 3H_2O + He$	$2.00 \times 10^{-37} (T_g/300)^{-2.5}$	[106] ^b
195	$H_2O^+ + O^- + He \rightarrow H_2O + O + He$	$2.00 \times 10^{-37} (T_g/300)^{-2.5}$	[106] ^b
196	$H_2O^+ + O_2^- + He \rightarrow H_2O + O_2 + He$	$2.00 \times 10^{-37} (T_g/300)^{-2.5}$	[106] ^b
197	$H_2O^+ + O_3^- + He \rightarrow H_2O + O_3 + He$	$2.00 \times 10^{-37} (T_g/300)^{-2.5}$	[106] ^b
198	$H_2O^+ + O_4^- + He \rightarrow H_2O + 2O_2 + He$	$2.00 \times 10^{-37} (T_g/300)^{-2.5}$	[106] ^b
199	$H_2O^+ + H^- + He \rightarrow H_2O + H + He$	$2.00 \times 10^{-37} (T_g/300)^{-2.5}$	[106] ^b
200	$H_2O^+ + OH^- + He \rightarrow H_2O + OH + He$	$2.00 \times 10^{-37} (T_g/300)^{-2.5}$	[106] ^b
201	$H_2O^+ + H_2O_2^- + He \rightarrow H_2O + H_2O_2 + He$	$2.00 \times 10^{-37} (T_g/300)^{-2.5}$	[106] ^b
202	$H_2O^+ + OH^-(H_2O) + He \rightarrow 2H_2O + OH + He$	$2.00 \times 10^{-37} (T_g/300)^{-2.5}$	[106] ^b
203	$H_2O^+ + OH^-(H_2O)_2 + He \rightarrow 3H_2O + OH + He$	$2.00 \times 10^{-37} (T_g/300)^{-2.5}$	[106] ^b
204	$H_2O^+ + OH^-(H_2O)_3 + He \rightarrow 4H_2O + OH + He$	$2.00 \times 10^{-37} (T_g/300)^{-2.5}$	[106] ^b
205	$H^+(H_2O) + O^- + He \rightarrow OH + H_2O + He$	$2.00 \times 10^{-37} (T_g/300)^{-2.5}$	[106] ^b
206	$H^+(H_2O) + O_2^- + He \rightarrow H + H_2O + O_2 + He$	$2.00 \times 10^{-37} (T_g/300)^{-2.5}$	[106] ^b
207	$H^+(H_2O) + O_3^- + He \rightarrow H + H_2O + O_3 + He$	$2.00 \times 10^{-37} (T_g/300)^{-2.5}$	[106] ^b
208	$H^+(H_2O) + O_4^- + He \rightarrow H + H_2O + 2O_2 + He$	$2.00 \times 10^{-37} (T_g/300)^{-2.5}$	[106] ^b
209	$H^+(H_2O) + H^- + He \rightarrow H_2 + H_2O + He$	$2.00 \times 10^{-37} (T_g/300)^{-2.5}$	[106] ^b
210	$H^+(H_2O) + OH^- + He \rightarrow 2H_2O + He$	$2.00 \times 10^{-37} (T_g/300)^{-2.5}$	[106] ^b
211	$H^+(H_2O) + H_2O_2^- + He \rightarrow 2H_2O + OH + He$	$2.00 \times 10^{-37} (T_g/300)^{-2.5}$	[106] ^b
212	$H^+(H_2O) + OH^-(H_2O) + He \rightarrow 3H_2O + He$	$2.00 \times 10^{-37} (T_g/300)^{-2.5}$	[106] ^b
213	$H^+(H_2O) + OH^-(H_2O)_2 + He \rightarrow 4H_2O + He$	$2.00 \times 10^{-37} (T_g/300)^{-2.5}$	[106] ^b
214	$H^+(H_2O) + OH^-(H_2O)_3 + He \rightarrow 5H_2O + He$	$2.00 \times 10^{-37} (T_g/300)^{-2.5}$	[106] ^b
215	$O_2^+(H_2O) + O^- + He \rightarrow O_2 + H_2O + O + He$	$2.00 \times 10^{-37} (T_g/300)^{-2.5}$	[106] ^b
216	$O_2^+(H_2O) + O_2^- + He \rightarrow 2O_2 + H_2O + He$	$2.00 \times 10^{-37} (T_g/300)^{-2.5}$	[106] ^b
217	$O_2^+(H_2O) + O_3^- + He \rightarrow O_2 + H_2O + O_3 + He$	$2.00 \times 10^{-37} (T_g/300)^{-2.5}$	[106] ^b
218	$O_2^+(H_2O) + O_4^- + He \rightarrow 3O_2 + H_2O + He$	$2.00 \times 10^{-37} (T_g/300)^{-2.5}$	[106] ^b
219	$O_2^+(H_2O) + H^- + He \rightarrow O_2 + H_2O + H + He$	$2.00 \times 10^{-37} (T_g/300)^{-2.5}$	[106] ^b
220	$O_2^+(H_2O) + OH^- + He \rightarrow O_2 + H_2O + OH + He$	$2.00 \times 10^{-37} (T_g/300)^{-2.5}$	[106] ^b
221	$O_2^+(H_2O) + H_2O_2^- + He \rightarrow O_2 + H_2O + H_2O_2 + He$	$2.00 \times 10^{-37} (T_g/300)^{-2.5}$	[106] ^b
222	$O_2^+(H_2O) + OH^-(H_2O) + He \rightarrow O_2 + 2H_2O + OH + He$	$2.00 \times 10^{-37} (T_g/300)^{-2.5}$	[106] ^b
223	$O_2^+(H_2O) + OH^-(H_2O)_2 + He \rightarrow O_2 + 3H_2O + OH + He$	$2.00 \times 10^{-37} (T_g/300)^{-2.5}$	[106] ^b
224	$O_2^+(H_2O) + OH^-(H_2O)_3 + He \rightarrow O_2 + 4H_2O + OH + He$	$2.00 \times 10^{-37} (T_g/300)^{-2.5}$	[106] ^b
225	$H_2O^+(H_2O) + O^- + He \rightarrow 2H_2O + O + He$	$2.00 \times 10^{-37} (T_g/300)^{-2.5}$	[106] ^b
226	$H_2O^+(H_2O) + O_2^- + He \rightarrow 2H_2O + O_2 + He$	$2.00 \times 10^{-37} (T_g/300)^{-2.5}$	[106] ^b
227	$H_2O^+(H_2O) + O_3^- + He \rightarrow 2H_2O + O_3 + He$	$2.00 \times 10^{-37} (T_g/300)^{-2.5}$	[106] ^b
228	$H_2O^+(H_2O) + O_4^- + He \rightarrow 2H_2O + 2O_2 + He$	$2.00 \times 10^{-37} (T_g/300)^{-2.5}$	[106] ^b
229	$H_2O^+(H_2O) + H^- + He \rightarrow 2H_2O + H + He$	$2.00 \times 10^{-37} (T_g/300)^{-2.5}$	[106] ^b
230	$H_2O^+(H_2O) + OH^- + He \rightarrow 2H_2O + OH + He$	$2.00 \times 10^{-37} (T_g/300)^{-2.5}$	[106] ^b

(Continued.)

No.	Reaction	Rate Coefficient ^a	Ref.
286	$H^+(H_2O)_7 + O_2^- + He \rightarrow 7H_2O + O_2 + H + He$	$2.00 \times 10^{-37} (T_g/300)^{-2.5}$	[106] ^b
287	$H^+(H_2O)_7 + O_3^- + He \rightarrow 7H_2O + O_3 + H + He$	$2.00 \times 10^{-37} (T_g/300)^{-2.5}$	[106] ^b
288	$H^+(H_2O)_7 + O_4^- + He \rightarrow 7H_2O + 2O_2 + H + He$	$2.00 \times 10^{-37} (T_g/300)^{-2.5}$	[106] ^b
289	$H^+(H_2O)_7 + H^- + He \rightarrow 7H_2O + H_2 + He$	$2.00 \times 10^{-37} (T_g/300)^{-2.5}$	[106] ^b
290	$H^+(H_2O)_7 + OH^- + He \rightarrow 8H_2O + He$	$2.00 \times 10^{-37} (T_g/300)^{-2.5}$	[106] ^b
291	$H^+(H_2O)_7 + H_2O_2^- + He \rightarrow 8H_2O + OH + He$	$2.00 \times 10^{-37} (T_g/300)^{-2.5}$	[106] ^b
292	$H^+(H_2O)_7 + OH^-(H_2O) + He \rightarrow 9H_2O + He$	$2.00 \times 10^{-37} (T_g/300)^{-2.5}$	[106] ^b
293	$H^+(H_2O)_7 + OH^-(H_2O)_2 + He \rightarrow 10H_2O + He$	$2.00 \times 10^{-37} (T_g/300)^{-2.5}$	[106] ^b
294	$H^+(H_2O)_7 + OH^-(H_2O)_3 + He \rightarrow 11H_2O + He$	$2.00 \times 10^{-37} (T_g/300)^{-2.5}$	[106] ^b
295	$H^+(H_2O)_8 + O^- + He \rightarrow 8H_2O + OH + He$	$2.00 \times 10^{-37} (T_g/300)^{-2.5}$	[106] ^b
296	$H^+(H_2O)_8 + O_2^- + He \rightarrow 8H_2O + O_2 + H + He$	$2.00 \times 10^{-37} (T_g/300)^{-2.5}$	[106] ^b
297	$H^+(H_2O)_8 + O_3^- + He \rightarrow 8H_2O + O_3 + H + He$	$2.00 \times 10^{-37} (T_g/300)^{-2.5}$	[106] ^b
298	$H^+(H_2O)_8 + O_4^- + He \rightarrow 8H_2O + 2O_2 + H + He$	$2.00 \times 10^{-37} (T_g/300)^{-2.5}$	[106] ^b
299	$H^+(H_2O)_8 + H^- + He \rightarrow 8H_2O + H_2 + He$	$2.00 \times 10^{-37} (T_g/300)^{-2.5}$	[106] ^b
300	$H^+(H_2O)_8 + OH^- + He \rightarrow 9H_2O + He$	$2.00 \times 10^{-37} (T_g/300)^{-2.5}$	[106] ^b
301	$H^+(H_2O)_8 + H_2O_2^- + He \rightarrow 9H_2O + OH + He$	$2.00 \times 10^{-37} (T_g/300)^{-2.5}$	[106] ^b
302	$H^+(H_2O)_8 + OH^-(H_2O) + He \rightarrow 10H_2O + He$	$2.00 \times 10^{-37} (T_g/300)^{-2.5}$	[106] ^b
303	$H^+(H_2O)_8 + OH^-(H_2O)_2 + He \rightarrow 11H_2O + He$	$2.00 \times 10^{-37} (T_g/300)^{-2.5}$	[106] ^b
304	$H^+(H_2O)_8 + OH^-(H_2O)_3 + He \rightarrow 12H_2O + He$	$2.00 \times 10^{-37} (T_g/300)^{-2.5}$	[106] ^b
305	$H^+(H_2O)_9 + O^- + He \rightarrow 9H_2O + OH + He$	$2.00 \times 10^{-37} (T_g/300)^{-2.5}$	[106] ^b
306	$H^+(H_2O)_9 + O_2^- + He \rightarrow 9H_2O + O_2 + H + He$	$2.00 \times 10^{-37} (T_g/300)^{-2.5}$	[106] ^b
307	$H^+(H_2O)_9 + O_3^- + He \rightarrow 9H_2O + O_3 + H + He$	$2.00 \times 10^{-37} (T_g/300)^{-2.5}$	[106] ^b
308	$H^+(H_2O)_9 + O_4^- + He \rightarrow 9H_2O + 2O_2 + H + He$	$2.00 \times 10^{-37} (T_g/300)^{-2.5}$	[106] ^b
309	$H^+(H_2O)_9 + H^- + He \rightarrow 9H_2O + H_2 + He$	$2.00 \times 10^{-37} (T_g/300)^{-2.5}$	[106] ^b
310	$H^+(H_2O)_9 + OH^- + He \rightarrow 10H_2O + He$	$2.00 \times 10^{-37} (T_g/300)^{-2.5}$	[106] ^b
311	$H^+(H_2O)_9 + H_2O_2^- + He \rightarrow 10H_2O + OH + He$	$2.00 \times 10^{-37} (T_g/300)^{-2.5}$	[106] ^b
312	$H^+(H_2O)_9 + OH^-(H_2O) + He \rightarrow 11H_2O + He$	$2.00 \times 10^{-37} (T_g/300)^{-2.5}$	[106] ^b
313	$H^+(H_2O)_9 + OH^-(H_2O)_2 + He \rightarrow 12H_2O + He$	$2.00 \times 10^{-37} (T_g/300)^{-2.5}$	[106] ^b
314	$H^+(H_2O)_9 + OH^-(H_2O)_3 + He \rightarrow 13H_2O + He$	$2.00 \times 10^{-37} (T_g/300)^{-2.5}$	[106] ^b

^a In $m^6 s^{-1}$.

^b Value estimated in reference.

No.	Reaction	Rate Coefficient ^a	Ref.
Two-body collisions—positive ions			
315	$He^+ + OH \rightarrow He + O^+ + H$	$1.10 \times 10^{-15} (T_g/300)^{-0.5}$	[94, 107]
316	$He^+ + H_2O \rightarrow He + OH^+ + H$	2.86×10^{-16}	[94, 108]
317	$He^+ + H_2O \rightarrow He + H_2O^+$	6.05×10^{-17}	[94, 108]
318	$He^+ + O \rightarrow He + O^+$	5.80×10^{-16}	[11, 109–111]
319	$He^+ + O(^1D) \rightarrow He + O^+$	5.80×10^{-16}	[11, 109–111]
320	$He^+ + O(^1S) \rightarrow He + O^+$	5.80×10^{-16}	[11, 109–111]
321	$He^+ + O_2 \rightarrow He + O^+ + O$	1.10×10^{-15}	[94, 112]
322	$He^+ + O_2 \rightarrow He + O_2^+$	3.30×10^{-17}	[94, 112]
323	$He^+ + O_2(a^1\Delta) \rightarrow He + O^+ + O$	1.10×10^{-15}	As reaction 321
324	$He^+ + O_2(a^1\Delta) \rightarrow He + O_2^+$	3.30×10^{-17}	As reaction 322
325	$He^+ + O_2(b^1\Sigma) \rightarrow He + O^+ + O$	1.10×10^{-15}	As reaction 321
326	$He^+ + O_2(b^1\Sigma) \rightarrow He + O_2^+$	3.30×10^{-17}	As reaction 322
327	$He^+ + O_3 \rightarrow He + O_2 + O^+$	2.20×10^{-15}	[11, 109–111]
328	$He_2^+ + OH \rightarrow 2He + O^+ + H$	1.10×10^{-15}	As reaction 315
329	$He_2^+ + H_2O \rightarrow 2He + H_2O^+$	6.05×10^{-17}	As reaction 317
330	$He_2^+ + H_2O \rightarrow 2He + OH^+ + H$	2.86×10^{-16}	As reaction 316
331	$He_2^+ + O \rightarrow 2He + O^+$	9.00×10^{-16}	[11, 109–111]

(Continued.)

No.	Reaction	Rate Coefficient ^a	Ref.
332	$\text{He}_2^+ + \text{O}(^1\text{D}) \rightarrow 2\text{He} + \text{O}^+$	9.00×10^{-16}	[11, 109–111]
333	$\text{He}_2^+ + \text{O}(^1\text{S}) \rightarrow 2\text{He} + \text{O}^+$	9.00×10^{-16}	[11, 109–111]
334	$\text{He}_2^+ + \text{O}_2 \rightarrow 2\text{He} + \text{O} + \text{O}^+$	1.00×10^{-16}	[11, 113]
335	$\text{He}_2^+ + \text{O}_2 \rightarrow 2\text{He} + \text{O}_2^+$	9.00×10^{-16}	[11, 113]
336	$\text{He}_2^+ + \text{O}_2(\text{a}^1\Delta) \rightarrow 2\text{He} + \text{O}_2^+$	1.20×10^{-15}	[[11]109–111]
337	$\text{He}_2^+ + \text{O}_2(\text{b}^1\Sigma) \rightarrow 2\text{He} + \text{O}_2^+$	1.20×10^{-15}	[11, 109–111]
338	$\text{He}_2^+ + \text{O}_3 \rightarrow 2\text{He} + \text{O}^+ + \text{O}_2$	1.60×10^{-15}	[[11]109–111]
339	$\text{OH}^+ + \text{H}_2 \rightarrow \text{H}_2\text{O}^+ + \text{H}$	1.01×10^{-15}	[94, 114]
340	$\text{OH}^+ + \text{OH} \rightarrow \text{H}_2\text{O}^+ + \text{O}$	$7.00 \times 10^{-16} (T_g/300)^{-0.5}$	[94, 107]
341	$\text{OH}^+ + \text{H}_2\text{O} \rightarrow \text{H}_2\text{O}^+ + \text{OH}$	1.56×10^{-15}	[115]
342	$\text{OH}^+ + \text{H}_2\text{O} \rightarrow \text{H}^+(\text{H}_2\text{O}) + \text{O}$	1.27×10^{-15}	[115]
343	$\text{OH}^+ + \text{O} \rightarrow \text{O}_2^+ + \text{H}$	7.10×10^{-16}	[94, 107]
344	$\text{OH}^+ + \text{O}(^1\text{D}) \rightarrow \text{O}_2^+ + \text{H}$	7.10×10^{-16}	As reaction 343
345	$\text{OH}^+ + \text{O}(^1\text{S}) \rightarrow \text{O}_2^+ + \text{H}$	7.10×10^{-16}	As reaction 343
346	$\text{OH}^+ + \text{O}_2 \rightarrow \text{O}_2^+ + \text{OH}$	5.90×10^{-16}	[94, 114]
347	$\text{OH}^+ + \text{O}_2(\text{a}^1\Delta) \rightarrow \text{O}_2^+ + \text{OH}$	5.90×10^{-16}	As reaction 346
348	$\text{OH}^+ + \text{O}_2(\text{b}^1\Sigma) \rightarrow \text{O}_2^+ + \text{OH}$	5.90×10^{-16}	As reaction 346
349	$\text{OH}^+ + \text{O}_3 \rightarrow \text{O}_3^+ + \text{OH}$	1.00×10^{-17}	Estimated
350	$\text{H}_2\text{O}^+ + \text{H}_2 \rightarrow \text{H}^+(\text{H}_2\text{O}) + \text{H}$	6.40×10^{-16}	[94, 116]
351	$\text{H}_2\text{O}^+ + \text{OH} \rightarrow \text{O} + \text{H}^+(\text{H}_2\text{O})$	$6.90 \times 10^{-16} (T_g/300)^{-0.5}$	[94, 107]
352	$\text{H}_2\text{O}^+ + \text{H}_2\text{O} \rightarrow \text{OH} + \text{H}^+(\text{H}_2\text{O})$	2.05×10^{-15}	[115]
353	$\text{H}_2\text{O}^+ + \text{O} \rightarrow \text{H}_2 + \text{O}_2^+$	4.00×10^{-17}	[94, 117]
354	$\text{H}_2\text{O}^+ + \text{O}(^1\text{D}) \rightarrow \text{H}_2 + \text{O}_2^+$	4.00×10^{-17}	As reaction 353
355	$\text{H}_2\text{O}^+ + \text{O}(^1\text{S}) \rightarrow \text{H}_2 + \text{O}_2^+$	4.00×10^{-17}	As reaction 353
356	$\text{H}_2\text{O}^+ + \text{O}_2 \rightarrow \text{H}_2\text{O} + \text{O}_2^+$	3.30×10^{-16}	[118]
357	$\text{H}_2\text{O}^+ + \text{O}_2(\text{a}^1\Delta) \rightarrow \text{H}_2\text{O} + \text{O}_2^+$	3.30×10^{-16}	As reaction 356
358	$\text{H}_2\text{O}^+ + \text{O}_2(\text{b}^1\Sigma) \rightarrow \text{H}_2\text{O} + \text{O}_2^+$	3.30×10^{-16}	As reaction 356
359	$\text{O}_2^+(\text{H}_2\text{O}) (+ \text{He}) \rightarrow \text{O}_2^+ + \text{H}_2\text{O} (+ \text{He})$	Effective	[119] ^{c,d}
360	$\text{O}_2^+(\text{H}_2\text{O}) + \text{H}_2\text{O} \rightarrow \text{O}_2 + \text{H}_2\text{O}^+(\text{H}_2\text{O})$	1.00×10^{-15}	[98] ^b
361	$\text{H}_2\text{O}^+(\text{H}_2\text{O}) + \text{H}_2\text{O} \rightarrow \text{OH} + \text{H}^+(\text{H}_2\text{O})_2$	1.40×10^{-15}	[98]
362	$\text{H}^+(\text{H}_2\text{O})_2 (+ \text{He}) \rightarrow \text{H}^+(\text{H}_2\text{O}) + \text{H}_2\text{O} (+ \text{He})$	Effective	[119] ^{c,d}
363	$\text{H}^+(\text{H}_2\text{O})_3 (+ \text{He}) \rightarrow \text{H}^+(\text{H}_2\text{O})_2 + \text{H}_2\text{O} (+ \text{He})$	Effective	[119] ^{c,d}
364	$\text{H}^+(\text{H}_2\text{O})_4 (+ \text{He}) \rightarrow \text{H}^+(\text{H}_2\text{O})_3 + \text{H}_2\text{O} (+ \text{He})$	Effective	[119] ^{c,d}
365	$\text{H}^+(\text{H}_2\text{O})_5 (+ \text{He}) \rightarrow \text{H}^+(\text{H}_2\text{O})_4 + \text{H}_2\text{O} (+ \text{He})$	Effective	[119] ^{c,d}
366	$\text{H}^+(\text{H}_2\text{O})_6 (+ \text{He}) \rightarrow \text{H}^+(\text{H}_2\text{O})_5 + \text{H}_2\text{O} (+ \text{He})$	Effective	[119] ^{c,d}
367	$\text{H}^+(\text{H}_2\text{O})_7 (+ \text{He}) \rightarrow \text{H}^+(\text{H}_2\text{O})_6 + \text{H}_2\text{O} (+ \text{He})$	Effective	[119] ^{c,d}
368	$\text{H}^+(\text{H}_2\text{O})_8 (+ \text{He}) \rightarrow \text{H}^+(\text{H}_2\text{O})_7 + \text{H}_2\text{O} (+ \text{He})$	Effective	[119] ^e
369	$\text{H}^+(\text{H}_2\text{O})_9 (+ \text{He}) \rightarrow \text{H}^+(\text{H}_2\text{O})_8 + \text{H}_2\text{O} (+ \text{He})$	Effective	[119] ^e
370	$\text{O}^+ + \text{H}_2 \rightarrow \text{OH}^+ + \text{H}$	1.70×10^{-15}	[94, 120]
371	$\text{O}^+ + \text{OH} \rightarrow \text{OH}^+ + \text{O}$	$3.60 \times 10^{-15} (T_g/300)^{-0.5}$	[94, 107]
372	$\text{O}^+ + \text{OH} \rightarrow \text{O}_2^+ + \text{H}$	$3.60 \times 10^{-15} (T_g/300)^{-0.5}$	[94, 107]
373	$\text{O}^+ + \text{H}_2\text{O} \rightarrow \text{O} + \text{H}_2\text{O}^+$	3.20×10^{-15}	[120]
374	$\text{O}^+ + \text{O}_2 \rightarrow \text{O} + \text{O}_2^+$	$2.00 \times 10^{-17} (T_g/300)^{-0.4}$	[121]
375	$\text{O}^+ + \text{O}_3 \rightarrow \text{O}_2 + \text{O}_2^+$	1.20×10^{-15}	[11, 109–111]
376	$\text{O}_2^+ + \text{He}(2^3\text{S}) \rightarrow \text{He} + \text{O} + \text{O}^+$	8.20×10^{-15}	[11, 109, 110, 122]
377	$\text{O}_3^+ + \text{He}(2^3\text{S}) \rightarrow \text{He} + \text{O} + \text{O}_2^+$	8.10×10^{-15}	[11, 109, 110, 122]
378	$\text{O}_3^+ + \text{O}(^1\text{D}) \rightarrow 2\text{O} + \text{O}_2^+$	3.00×10^{-16}	[11, 109–111]
379	$\text{O}_3^+ + \text{O}(^1\text{S}) \rightarrow 2\text{O} + \text{O}_2^+$	2.00×10^{-16}	[11, 109–111]
380	$\text{O}_3^+ + \text{O}_2 \rightarrow \text{O}_2^+ + \text{O}_3$	6.70×10^{-16}	[11, 109–111, 123]
381	$\text{O}_4^+ + \text{He} \rightarrow \text{O}_2^+ + \text{O}_2 + \text{He}$	3.40×10^{-20}	[11, 113]
382	$\text{O}_4^+ + \text{He}(2^3\text{S}) \rightarrow \text{He} + \text{O}_2 + \text{O}_2^+$	8.00×10^{-15}	[11, 109, 110, 122]
383	$\text{O}_4^+ + \text{H}_2\text{O} \rightarrow \text{O}_2 + \text{O}_2^+\text{H}_2\text{O}$	1.70×10^{-15}	[124]
384	$\text{O}_4^+ + \text{O} \rightarrow \text{O}_3 + \text{O}_2^+$	3.00×10^{-16}	[98]
385	$\text{O}_4^+ + \text{O}(^1\text{D}) \rightarrow \text{O} + \text{O}_2 + \text{O}_2^+$	3.00×10^{-16}	[11, 109, 110, 125]
386	$\text{O}_4^+ + \text{O}(^1\text{D}) \rightarrow \text{O}_3 + \text{O}_2^+$	3.00×10^{-16}	[11, 109, 110, 125]
387	$\text{O}_4^+ + \text{O}(^1\text{S}) \rightarrow \text{O} + \text{O}_2 + \text{O}_2^+$	3.00×10^{-16}	[11, 109, 110, 125]

(Continued.)

No.	Reaction	Rate Coefficient ^a	Ref.
388	$O_4^+ + O(^1S) \rightarrow O_2^+ + O_3$	3.00×10^{-16}	[11, 109, 110, 125]
389	$O_4^+ + O_2 \rightarrow 2O_2 + O_2^+$	$1.00 \times 10^{-11} (T_g/300)^{-4.2} e^{-5400/T_g}$	[11, 98, 113]
390	$O_4^+ + O_2(a^1\Delta) \rightarrow 2O_2 + O_2^+$	6.00×10^{-16}	[11, 109–111]
391	$O_4^+ + O_2(b^1\Sigma) \rightarrow 2O_2 + O_2^+$	6.00×10^{-16}	[11]
Two-body collisions—negative ions			
392	$H^- + He \rightarrow He + H + e$	$4.43 \times 10^{-17} e^{-5829/T_g}$	[126]
393	$H^- + H \rightarrow H_2 + e$	$4.32 \times 10^{-15} (T_g/300)^{-0.39} e^{-39.4/T_g}$	[127]
394	$H^- + H_2O \rightarrow OH^- + H_2$	4.80×10^{-15}	[94, 128]
395	$H^- + O \rightarrow OH + e$	1.00×10^{-15}	[107]
396	$H^- + OH \rightarrow H_2O + e$	1.00×10^{-16}	[107]
397	$OH^- + H \rightarrow H_2O + e$	1.40×10^{-15}	[94, 129]
398	$H_2O_2^- + H_2O \rightarrow OH^-(H_2O) + OH$	1.00×10^{-17}	[130] ^f
399	$O^- + He \rightarrow e + He + O$	$2.50 \times 10^{-24} (T_g/300)^{0.6}$	[11, 42, 131]
400	$O^- + He(2^3S) \rightarrow 2e + He + O^+$	8.70×10^{-15}	[11, 109, 110, 122]
401	$O^- + H_2O \rightarrow OH^- + OH$	1.40×10^{-15}	[83]
402	$O^- + O \rightarrow e + O_2$	$2.30 \times 10^{-16} (T_g/300)^{-1.3}$	[132, 133]
403	$O^- + O(^1D) \rightarrow 2O + e$	7.40×10^{-16}	[11, 109, 110, 125]
404	$O^- + O(^1S) \rightarrow e + 2O$	7.40×10^{-16}	[11, 109, 110, 125]
405	$O^- + O_2 \rightarrow O_3 + e$	1.00×10^{-18}	[11, 113]
406	$O^- + O_2 \rightarrow O_2^- + O$	1.00×10^{-18}	[11, 113]
407	$O^- + O_2(a^1\Delta) \rightarrow O_2^- + O$	$7.90 \times 10^{-16} e^{-890/T_g}$	[11, 134]
408	$O^- + O_2(a^1\Delta) \rightarrow O_3 + e$	6.10×10^{-16}	[11, 134]
409	$O^- + O_2(b^1\Sigma) \rightarrow O_2^- + O$	$7.90 \times 10^{-16} e^{-890/T_g}$	As reaction 407
410	$O^- + O_2(b^1\Sigma) \rightarrow O_3 + e$	6.10×10^{-16}	As reaction 408
411	$O^- + O_3 \rightarrow e + 2O_2$	3.00×10^{-16}	[11, 113, 135]
412	$O^- + O_3 \rightarrow O + O_3^-$	2.00×10^{-16}	[11, 113, 135]
413	$O^- + O_3 \rightarrow O_2^- + O_2$	1.00×10^{-17}	[11, 113, 135]
414	$O_2^- + He \rightarrow e + He + O_2$	$3.90 \times 10^{-16} e^{-7400/T_g}$	[11, 136]
415	$O_2^- + He(2^3S) \rightarrow 2e + He + O_2^+$	8.30×10^{-15}	[11, 109, 110, 122]
416	$O_2^- + O \rightarrow O^- + O_2$	$8.50 \times 10^{-17} (T_g/300)^{-1.8}$	[133] ^g
417	$O_2^- + O \rightarrow O_3 + e$	$8.50 \times 10^{-17} (T_g/300)^{-1.8}$	[133] ^g
418	$O_2^- + O(^1D) \rightarrow e + O_3$	$8.50 \times 10^{-17} (T_g/300)^{-1.8}$	[11]
419	$O_2^- + O(^1D) \rightarrow O^- + O_2$	$8.50 \times 10^{-17} (T_g/300)^{-1.8}$	[11]
420	$O_2^- + O(^1S) \rightarrow O^- + O_2$	$8.50 \times 10^{-17} (T_g/300)^{-1.8}$	[11]
421	$O_2^- + O(^1S) \rightarrow e + O_3$	$8.50 \times 10^{-17} (T_g/300)^{-1.8}$	[11]
422	$O_2^- + O_2 \rightarrow e + 2O_2$	$2.70 \times 10^{-16} (T_g/300)^{0.5} e^{-5590/T_g}$	[98]
423	$O_2^- + O_2 \rightarrow O + O_3^-$	3.50×10^{-21}	[113]
424	$O_2^- + O_2(a^1\Delta) \rightarrow e + 2O_2$	7.00×10^{-16}	[134]
425	$O_2^- + O_2(b^1\Sigma) \rightarrow e + 2O_2$	7.00×10^{-16}	[11]
426	$O_2^- + O_3 \rightarrow O_2 + O_3^-$	6.00×10^{-16}	[113]
427	$O_3^- + He(2^3S) \rightarrow 2e + He + O + O_2^+$	8.10×10^{-15}	[11, 109, 110, 122]
428	$O_3^- + O \rightarrow e + 2O_2$	1.00×10^{-17}	[98]
429	$O_3^- + O \rightarrow O_2 + O_2^-$	2.50×10^{-16}	[113]
430	$O_3^- + O(^1D) \rightarrow O + O_2 + O^-$	3.00×10^{-16}	[11, 109–111]
431	$O_3^- + O(^1D) \rightarrow O + O_3 + e$	3.00×10^{-16}	[11, 109, 110, 125]
432	$O_3^- + O(^1S) \rightarrow e + O + O_3$	2.00×10^{-16}	[11, 109–111]
433	$O_3^- + O(^1S) \rightarrow 2O + O_2^-$	2.00×10^{-16}	[11, 109–111]
434	$O_3^- + O(^1S) \rightarrow O + O^- + O_2$	2.00×10^{-16}	[11, 109–111]
435	$O_3^- + O_2(b^1\Sigma) \rightarrow O^- + 2O_2$	$6.70 \times 10^{-16} e^{-1300/T_g}$	[11, 109–111]
436	$O_3^- + O_3 \rightarrow e + 3O_2$	8.50×10^{-16}	[11, 109–111]
437	$O_4^- + He \rightarrow He + O_2 + O_2^-$	$2.20 \times 10^{-11} (T_g/300)^{-1} e^{-6300/T_g}$	[98]
438	$O_4^- + He(2^3S) \rightarrow 2e + He + O_2 + O_2^+$	8.00×10^{-15}	[11, 109, 110, 122]
439	$O_4^- + O \rightarrow O_2 + O_3^-$	4.00×10^{-16}	[98, 113]

(Continued.)

No.	Reaction	Rate Coefficient ^a	Ref.
440	$O_4^- + O(^1D) \rightarrow e + O + 2O_2$	2.00×10^{-16}	[11, 109–111]
441	$O_4^- + O(^1D) \rightarrow O + O_2 + O_2^-$	2.00×10^{-16}	[11, 109–111]
442	$O_4^- + O(^1D) \rightarrow 2O_2 + O^-$	2.00×10^{-16}	[[11]109–111]
443	$O_4^- + O(^1S) \rightarrow e + O + 2O_2$	2.00×10^{-16}	[11, 109–111]
444	$O_4^- + O(^1S) \rightarrow O + O_2 + O_2^-$	2.00×10^{-16}	[11, 109–111]
445	$O_4^- + O(^1S) \rightarrow O^- + 2O_2$	2.00×10^{-16}	[11, 109–111]
446	$O_4^- + O_2 \rightarrow 2O_2 + O_2^-$	$2.20 \times 10^{-11} (T_g/300)^{-1} e^{-6300/T_g}$	[98]
447	$O_4^- + O_2(a^1\Delta) \rightarrow 3O_2 + e$	3.00×10^{-16}	[11, 109–111]
448	$O_4^- + O_2(a^1\Delta) \rightarrow 2O_2 + O_2^-$	3.00×10^{-16}	[11, 109–111]
449	$O_4^- + O_2(b^1\Sigma) \rightarrow e + 3O_2$	3.00×10^{-16}	[11, 109–111]
450	$O_4^- + O_2(b^1\Sigma) \rightarrow 2O_2 + O_2^-$	3.00×10^{-16}	[11, 109–111]
451	$O_4^- + O_3 \rightarrow 2O_2 + O_3^-$	8.00×10^{-16}	[11, 109–111]
Three-body collisions—positive ions			
454	$He^+ + 2He \rightarrow He + He_2^+$	$1.30 \times 10^{-43} (T_g/300)^{-0.6}$	[137]
455	$H^+(H_2O) + H_2O (+ He) \rightarrow H^+(H_2O)_2 (+ He)$	Effective	[119, 138] ^{c,d}
456	$H^+(H_2O)_2 + H_2O (+ He) \rightarrow H^+(H_2O)_3 (+ He)$	Effective	[119, 138] ^{c,d}
457	$H^+(H_2O)_3 + H_2O (+ He) \rightarrow H^+(H_2O)_4 (+ He)$	Effective	[119, 138] ^{c,d}
458	$H^+(H_2O)_4 + H_2O (+ He) \rightarrow H^+(H_2O)_5 (+ He)$	Effective	[119, 138] ^{c,d}
459	$H^+(H_2O)_5 + H_2O (+ He) \rightarrow H^+(H_2O)_6 (+ He)$	Effective	[119, 138] ^{c,d}
458	$H^+(H_2O)_6 + H_2O (+ He) \rightarrow H^+(H_2O)_7 (+ He)$	Effective	[119, 138] ^{c,d}
459	$H^+(H_2O)_7 + H_2O (+ He) \rightarrow H^+(H_2O)_8 (+ He)$	Effective	[119] ^e
460	$H^+(H_2O)_8 + H_2O (+ He) \rightarrow H^+(H_2O)_9 (+ He)$	Effective	[119] ^e
461	$He + O_2 + O_2^+ \rightarrow He + O_4^+$	$5.50 \times 10^{-43} (T_g/300)^{-2.7}$	[113, 139]
462	$O_2^+ + H_2O (+ He) \rightarrow O_2^+(H_2O) (+ He)$	Effective	[119] ^{c,d}
463	$He + O + O^+ \rightarrow He + O_2^+$	$5.50 \times 10^{-43} (T_g/300)^{-2.7}$	[11]
Three-body collisions—negative ions			
464	$OH^- + H_2O + He \rightarrow OH^-(H_2O) + He$	8.00×10^{-42}	[140] ^h
465	$OH^-(H_2O) + H_2O + He \rightarrow OH^-(H_2O)_2 + He$	2.50×10^{-43}	[140] ^h
466	$OH^-(H_2O)_2 + H_2O + He \rightarrow OH^-(H_2O)_3 + He$	1.50×10^{-43}	[140] ^h
467	$O^- + H_2O + He \rightarrow H_2O_2^- + He$	1.30×10^{-40}	[130]
468	$O^- + O_2 + He \rightarrow He + O_3^-$	$3.70 \times 10^{-43} (T_g/300)^{-1}$	[98, 141]
469	$He + O_2 + O_2^- \rightarrow He + O_4^-$	$1.20 \times 10^{-43} (T_g/300)^{-2.7}$	[98, 141]

^a In s^{-1} , $m^3 s^{-1}$ and $m^6 s^{-1}$ for one-, two- and three-body reactions, respectively.

^b Value is estimated in reference.

^c Effective rate coefficients calculated from pressure dependent rates as described by Sieck *et al* [119] for 1 atm and a temperature range 280–350 K.

^d Background gas is (humid) air in given reference. Gas efficiency factors for He background gas are not known for these reactions, but could potentially change calculated reaction rate coefficients if taken into account.

^e Rate coefficients are estimated by extrapolating the coefficients k_0^{300} and A given by Sieck *et al* [119] using an exponential fit, and using constant values $n = 16$, $B = 5000$, and $k_L = 10^{-24}$.

^f Value is listed as a lower limit in reference.

^g Estimated branching ratio.

^h Third body is H_2O in reference.

No.	Reaction	Rate Coefficient ^a	Ref.
Two-body collisions			
470	He + O(¹ D) → He + O	7.00×10^{-22}	[142] ^b
471	He + O(¹ S) → He + O	7.00×10^{-22}	As reaction 470
472	He + O ₂ (a ¹ Δ) → He + O ₂	5.00×10^{-27}	[143]
473	He + O ₂ (b ¹ Σ) → He + O ₂ (a ¹ Δ)	$1.00 \times 10^{-23} (T_g/300)^{0.5}$	[144] ^c
474	He + O ₃ → He + O + O ₂	$5.61 \times 10^{-16} e^{-11400/T_g}$	[141]
475	2He(2 ³ S) → He + He ⁺ + e	4.50×10^{-16}	[73, 145]
476	2He(2 ³ S) → He ₂ ⁺ + e	1.05×10^{-15}	[73, 145]
477	He(2 ³ S) + He ₂ [*] → 2He + He ⁺ + e	5.00×10^{-16}	[73] ^d
478	He(2 ³ S) + He ₂ [*] → He + He ₂ ⁺ + e	2.00×10^{-15}	[73] ^d
479	He(2 ³ S) + H ₂ O → He + OH ⁺ + H + e	1.39×10^{-16}	[146, 147] ^e
480	He(2 ³ S) + OH → OH ⁺ + He + e	6.08×10^{-16}	As reaction 481
481	He(2 ³ S) + H ₂ O → He + H ₂ O ⁺ + e	6.08×10^{-16}	[146, 147] ^e
482	He(2 ³ S) + H ₂ O ₂ → He + OH ⁺ + OH + e	6.08×10^{-16}	As reaction 481
483	He(2 ³ S) + O ₂ → He + O ₂ ⁺ + e	2.54×10^{-16}	[148]
484	He(2 ³ S) + O(¹ D) → He + O ⁺ + e	2.54×10^{-16}	As reaction 483
485	He(2 ³ S) + O(¹ S) → He + O ⁺ + e	2.54×10^{-16}	As reaction 483
486	He(2 ³ S) + O → He + O ⁺ + e	2.54×10^{-16}	As reaction 483
487	He(2 ³ S) + O ₂ (a ¹ Δ) → He + O ₂ ⁺ + e	2.54×10^{-16}	As reaction 483
488	He(2 ³ S) + O ₂ (b ¹ Σ) → He + O ₂ ⁺ + e	2.54×10^{-16}	As reaction 483
489	He(2 ³ S) + O ₃ → He + O ₂ ⁺ + O + e	2.60×10^{-16}	[11] ^c
490	He ₂ [*] + He ₂ [*] → e + He ⁺ + 3He	3.00×10^{-16}	[73, 149]
491	He ₂ [*] + He ₂ [*] → e + 2He + He ₂ ⁺	1.20×10^{-15}	[73, 149]
492	He ₂ [*] + H ₂ O → 2He + H ₂ O ⁺ + e	2.20×10^{-15}	[150]
493	He ₂ [*] + O → 2He + O ⁺ + e	3.60×10^{-16}	As reaction 496
494	He ₂ [*] + O(¹ D) → 2He + O ⁺ + e	3.60×10^{-16}	As reaction 496
495	He ₂ [*] + O(¹ S) → 2He + O ⁺ + e	3.60×10^{-16}	As reaction 496
496	He ₂ [*] + O ₂ → 2He + O ₂ ⁺ + e	3.60×10^{-16}	[150]
497	He ₂ [*] + O ₂ (a ¹ Δ) → 2He + O ₂ ⁺ + e	3.60×10^{-16}	As reaction 496
498	He ₂ [*] + O ₂ (b ¹ Σ) → 2He + O ₂ ⁺ + e	3.60×10^{-16}	As reaction 496
499	He ₂ [*] + O ₃ → 2He + O ₂ ⁺ + O + e	3.60×10^{-16}	As reaction 496
500	H + OH → H ₂ + O	$6.86 \times 10^{-20} (T_g/300)^{2.8} e^{-1950/T_g}$	[151]
501	H + HO ₂ → O ₂ + H ₂	5.60×10^{-18}	[152]
502	H + HO ₂ → 2OH	7.20×10^{-17}	[152]
503	H + HO ₂ → H ₂ O + O	2.40×10^{-18}	[152]
504	H + H ₂ O ₂ → H ₂ O + OH	$1.70 \times 10^{-17} e^{-1800/T_g}$	[153]
505	H + H ₂ O ₂ → H ₂ + HO ₂	$2.80 \times 10^{-18} e^{-1890/T_g}$	[153]
506	H + O ₃ → O ₂ + OH	$1.40 \times 10^{-16} e^{-470/T_g}$	[154, 155]
507	H ₂ + OH → H ₂ O + H	$4.27 \times 10^{-19} (T_g/300)^{2.41} e^{-1240/T_g}$	[156]
508	H ₂ + O(¹ D) → OH + H	1.20×10^{-16}	[152]
509	H ₂ + O(¹ S) → OH + H	1.20×10^{-16}	As reaction 508
510	2OH → O + H ₂ O	$6.20 \times 10^{-20} (T_g/300)^{2.6} e^{945/T_g}$	[152]
511	OH + HO ₂ → O ₂ + H ₂ O	$4.80 \times 10^{-17} e^{250/T_g}$	[152, 157, 158]
512	OH + H ₂ O ₂ → HO ₂ + H ₂ O	$2.90 \times 10^{-18} e^{-160/T_g}$	[152]
513	OH + O → O ₂ + H	$2.40 \times 10^{-17} e^{110/T_g}$	[152, 159, 160]
514	OH + O(¹ D) → O ₂ + H	$2.40 \times 10^{-17} e^{110/T_g}$	As reaction 513
515	OH + O(¹ S) → O ₂ + H	$2.40 \times 10^{-17} e^{110/T_g}$	As reaction 513
516	OH + O ₃ → O ₂ + HO ₂	$1.70 \times 10^{-18} e^{-940/T_g}$	[152]
517	H ₂ O + O(¹ D) → 2OH	$1.63 \times 10^{-16} e^{60/T_g}$	[154]
518	H ₂ O + O(¹ S) → O + H ₂ O	4.50×10^{-17}	[161]
519	H ₂ O + O(¹ S) → O(¹ D) + H ₂ O	1.50×10^{-16}	[161]
520	H ₂ O + O(¹ S) → 2OH	3.05×10^{-16}	[161]
521	H ₂ O + O ₂ (a ¹ Δ) → O ₂ + H ₂ O	4.80×10^{-24}	[154]

(Continued.)

No.	Reaction	Rate Coefficient ^a	Ref.
522	$\text{H}_2\text{O} + \text{O}_2(\text{b}^1\Sigma) \rightarrow \text{O}_2 + \text{H}_2\text{O}$	$3.90 \times 10^{-18} e^{125/Tg}$	[154]
523	$\text{HO}_2 + \text{O} \rightarrow \text{OH} + \text{O}_2$	$2.70 \times 10^{-17} e^{224/Tg}$	[152, 157]
524	$\text{H}_2\text{O}_2 + \text{O}(\text{D}) \rightarrow \text{H}_2\text{O} + \text{O}_2$	5.20×10^{-16}	[162]
525	$\text{H}_2\text{O}_2 + \text{O}(\text{S}) \rightarrow \text{H}_2\text{O} + \text{O}_2$	5.20×10^{-16}	As reaction 524
526	$\text{HO}_2 + \text{O}(\text{D}) \rightarrow \text{OH} + \text{O}_2$	5.20×10^{-16}	As reaction 524
527	$\text{HO}_2 + \text{O}(\text{S}) \rightarrow \text{OH} + \text{O}_2$	5.20×10^{-16}	As reaction 524
528	$\text{O} + \text{O}(\text{D}) \rightarrow 2\text{O}$	8.00×10^{-18}	[163]
529	$\text{O} + \text{O}(\text{S}) \rightarrow 2\text{O}$	$3.33 \times 10^{-17} e^{-300/Tg}$	[144, 164] ^d
530	$\text{O} + \text{O}(\text{S}) \rightarrow \text{O} + \text{O}(\text{D})$	$1.67 \times 10^{-17} e^{-300/Tg}$	[144, 164] ^d
531	$\text{O} + \text{O}_2(\text{a}^1\Delta) \rightarrow \text{O} + \text{O}_2$	1.00×10^{-22}	[154]
532	$\text{O} + \text{O}_2(\text{b}^1\Sigma) \rightarrow \text{O} + \text{O}_2(\text{a}^1\Delta)$	8.00×10^{-20}	[152, 154]
533	$\text{O} + \text{O}_3 \rightarrow 2\text{O} + \text{O}_2$	$1.20 \times 10^{-15} e^{-11400/Tg}$	[141]
534	$\text{O} + \text{O}_3 \rightarrow 2\text{O}_2$	$8.00 \times 10^{-18} e^{-2060/Tg}$	[11, 152, 154, 165]
535	$\text{O}(\text{D}) + \text{O}_2 \rightarrow \text{O} + \text{O}_2(\text{b}^1\Sigma)$	$2.56 \times 10^{-17} e^{67/Tg}$	[152]
536	$\text{O}(\text{D}) + \text{O}_2 \rightarrow \text{O} + \text{O}_2(\text{a}^1\Delta)$	$6.60 \times 10^{-18} e^{55/Tg}$	[154]
537	$\text{O}(\text{D}) + \text{O}_3 \rightarrow 2\text{O}_2$	1.20×10^{-16}	[152]
538	$\text{O}(\text{D}) + \text{O}_3 \rightarrow \text{O}_2 + 2\text{O}$	1.20×10^{-16}	[152]
539	$\text{O}(\text{S}) + \text{O}_2 \rightarrow \text{O} + \text{O}_2$	$3.00 \times 10^{-18} e^{-850/Tg}$	[11, 98, 161]
540	$\text{O}(\text{S}) + \text{O}_2 \rightarrow \text{O}(\text{D}) + \text{O}_2$	$1.30 \times 10^{-18} e^{-850/Tg}$	[11, 98, 161]
541	$\text{O}(\text{S}) + \text{O}_2(\text{a}^1\Delta) \rightarrow 3\text{O}$	3.20×10^{-17}	[11, 166–168]
542	$\text{O}(\text{S}) + \text{O}_2(\text{a}^1\Delta) \rightarrow \text{O} + \text{O}_2(\text{b}^1\Sigma)$	1.30×10^{-16}	[11, 166–168]
543	$\text{O}(\text{S}) + \text{O}_2(\text{a}^1\Delta) \rightarrow \text{O}(\text{D}) + \text{O}_2$	3.60×10^{-17}	[11, 166, 167]
544	$\text{O}(\text{S}) + \text{O}_3 \rightarrow \text{O} + \text{O}(\text{D}) + \text{O}_2$	1.93×10^{-16}	[169]
545	$\text{O}(\text{S}) + \text{O}_3 \rightarrow 2\text{O}_2$	1.93×10^{-16}	[169]
546	$\text{O}(\text{S}) + \text{O}_3 \rightarrow 2\text{O} + \text{O}_2$	1.93×10^{-16}	[169]
547	$2\text{O}_2 \rightarrow 2\text{O} + \text{O}_2$	$6.60 \times 10^{-15} (T_g/300)^{-1.5} e^{-59000/Tg}$	[98]
548	$\text{O}_2 + \text{O}_2(\text{a}^1\Delta) \rightarrow \text{O}_2\text{O}_2$	$3.00 \times 10^{-24} e^{-200/Tg}$	[152]
549	$\text{O}_2 + \text{O}_2(\text{b}^1\Sigma) \rightarrow \text{O}_2 + \text{O}_2(\text{a}^1\Delta)$	$3.60 \times 10^{-23} (T_g/300)^{0.5}$	[144]
550	$\text{O}_2 + \text{O}_3 \rightarrow \text{O} + 2\text{O}_2$	$7.26 \times 10^{-16} e^{-11435/Tg}$	[169]
551	$2\text{O}_2(\text{a}^1\Delta) \rightarrow \text{O}_2 + \text{O}_2(\text{b}^1\Sigma)$	$1.80 \times 10^{-24} (T_g/300)^{3.8} e^{700/Tg}$	[170, 171]
552	$\text{O}_2(\text{a}^1\Delta) + \text{O}_2(\text{b}^1\Sigma) \rightarrow \text{O}_2 + \text{O}_2(\text{b}^1\Sigma)$	2.70×10^{-23}	[11]
553	$\text{O}_2(\text{a}^1\Delta) + \text{O}_3 \rightarrow 2\text{O}_2 + \text{O}$	$5.20 \times 10^{-17} e^{-2840/Tg}$	[154]
554	$2\text{O}_2(\text{b}^1\Sigma) \rightarrow \text{O}_2 + \text{O}_2(\text{b}^1\Sigma)$	2.70×10^{-23}	[11]
555	$\text{O}_2(\text{b}^1\Sigma) + \text{O}_3 \rightarrow 2\text{O}_2 + \text{O}$	$3.50 \times 10^{-17} e^{-135/Tg}$	[154]
556	$\text{O}_2(\text{b}^1\Sigma) + \text{O}_3 \rightarrow \text{O}_2 + \text{O}_3$	$5.50 \times 10^{-18} e^{-135/Tg}$	[11, 154]
557	$\text{O}_2(\text{b}^1\Sigma) + \text{O}_3 \rightarrow \text{O}_2(\text{a}^1\Delta) + \text{O}_3$	$5.50 \times 10^{-18} e^{-135/Tg}$	[11, 154]
558	$2\text{O}_3 \rightarrow \text{O} + \text{O}_2 + \text{O}_3$	$1.65 \times 10^{-15} e^{-11435/Tg}$	[169]
Three-body collisions			
559	$2\text{He} + \text{He}(2^3\text{S}) \rightarrow \text{He} + \text{He}_2^*$	2.00×10^{-46}	[172]
560	$\text{He} + \text{He}(2^3\text{S}) + \text{H}_2\text{O} \rightarrow 2\text{He} + \text{H}_2\text{O}^+ + \text{e}$	1.48×10^{-41}	[146] ^c
561	$\text{He} + \text{He}(2^3\text{S}) + \text{O} \rightarrow \text{e} + 2\text{He} + \text{O}^+$	1.60×10^{-43}	[11]
562	$\text{He} + \text{He}(2^3\text{S}) + \text{O}(\text{D}) \rightarrow \text{e} + 2\text{He} + \text{O}^+$	1.60×10^{-43}	[11]
563	$\text{He} + \text{He}(2^3\text{S}) + \text{O}(\text{S}) \rightarrow \text{e} + 2\text{He} + \text{O}^+$	1.60×10^{-43}	[11]
564	$\text{He} + \text{He}(2^3\text{S}) + \text{O}_2 \rightarrow \text{e} + 2\text{He} + \text{O}_2^+$	1.60×10^{-43}	[148]
565	$\text{He} + \text{He}(2^3\text{S}) + \text{O}_2(\text{a}^1\Delta) \rightarrow \text{e} + 2\text{He} + \text{O}_2^+$	1.60×10^{-43}	[11]
566	$\text{He} + \text{He}(2^3\text{S}) + \text{O}_2(\text{b}^1\Sigma) \rightarrow \text{e} + 2\text{He} + \text{O}_2^+$	1.60×10^{-43}	[11]
567	$\text{He} + \text{He}(2^3\text{S}) + \text{O}_3 \rightarrow \text{e} + 2\text{He} + \text{O} + \text{O}_2^+$	1.60×10^{-43}	[11]
568	$\text{He} + 2\text{H} \rightarrow \text{He} + \text{H}_2$	$6.04 \times 10^{-45} (T_g/300)^{-1}$	[153, 173] ^f
569	$\text{He} + \text{H} + \text{OH} \rightarrow \text{He} + \text{H}_2\text{O}$	$9.23 \times 10^{-44} (T_g/300)^{-1.527} e^{-185/Tg}$	[174, 175] ^g
570	$\text{He} + \text{H} + \text{O} \rightarrow \text{OH} + \text{He}$	$4.36 \times 10^{-44} (T_g/300)^{-1}$	[151] ^c
571	$\text{H} + \text{O}_2 (+ \text{He}) \rightarrow \text{HO}_2 (+ \text{He})$	Effective	[152, 176] ^{h,i}
572	$2\text{OH} (+ \text{He}) \rightarrow \text{H}_2\text{O}_2 (+ \text{He})$	Effective	[152] ^{h,j}
573	$\text{He} + 2\text{O} \rightarrow \text{He} + \text{O}_2(\text{a}^1\Delta)$	$2.00 \times 10^{-45} (T_g/300)^{-1} e^{-170/Tg}$	[11, 141, 177]

(Continued.)

No.	Reaction	Rate Coefficient ^a	Ref.
574	He + 2O → He + O ₂ (b ¹ Σ)	$2.00 \times 10^{-45} (T_g/300)^{-1} e^{-170/T_g}$	[11, 141, 177]
575	He + O + O ₂ → He + O ₃	$3.66 \times 10^{-46} (T_g/300)^{-2.6}$	[152, 178] ^k
576	He + O + O ₂ (a ¹ Δ) → He + O ₂ + O	4.00×10^{-45}	[179, 180]

^a In m³ s⁻¹ and m⁶ s⁻¹ for two- and three-body collisions, respectively.

^b Value is an upper limit in reference.

^c Estimated value in reference.

^d Estimated branching ratio.

^e Branching ratios taken from Sanders [147].

^f Third body is Ar instead of He in reference. The gas efficiency factor is assumed to be 1.

^g Third body is Ar instead of He in reference. The gas efficiency factor is assumed to be 0.65. This factor is calculated by dividing reaction rate coefficients for He and Ar as background gases for the same reaction measured by Zellner *et al* [175].

^h Effective rate coefficients calculated from pressure dependent rates for 1 atm and fitted by an Arrhenius expression in the temperature range 280–350 K.

ⁱ Third body is N₂ instead of He in reference. The gas efficiency factor is assumed to be 0.43. This factor is calculated by dividing reaction rate coefficients for He and N₂ as background gases for the same reaction measured by Hsu *et al* [176].

^j Recommended rate coefficient in reference is for N₂ background gas instead of He. We apply a gas efficiency factor of 0.41 to the low-pressure limit reaction rate coefficient to account for this. This factor is calculated by dividing the room temperature rate coefficient from the given reference for He background gas (measured by Forster *et al* [181]) by the recommended value (measured by Fulle *et al* [182]).

^k Third body is N₂ instead of He in reference. The gas efficiency factor is assumed to be 0.61. This factor is calculated by dividing reaction rate coefficients for He and N₂ as background gases for the same reaction measured by Lin and Leu [178].

ORCID iDs

Alexandra Brisset  <https://orcid.org/0000-0003-3217-1106>

Andrew R Gibson  <https://orcid.org/0000-0002-1082-4359>

Sandra Schröter  <https://orcid.org/0000-0003-1029-4041>

Kari Niemi  <https://orcid.org/0000-0001-6134-1974>

Jean-Paul Booth  <https://orcid.org/0000-0002-0980-3278>

Timo Gans  <https://orcid.org/0000-0003-1362-8000>

Deborah O'Connell  <https://orcid.org/0000-0002-1457-9004>

Erik Wagenaars  <https://orcid.org/0000-0002-5493-3434>

References

- [1] Graves D B 2012 The emerging role of reactive oxygen and nitrogen species in redox biology and some implications for plasma applications to medicine and biology *J. Phys. D: Appl. Phys.* **45** 263001
- [2] Lu X, Naidis G V, Laroussi M, Reuter S, Graves D B and Ostrikov K 2016 Reactive species in non-equilibrium atmospheric-pressure plasmas: generation, transport, and biological effects *Phys. Rep.* **630** 1–84
- [3] Invernizzi L, Muja C, Sainct F P and Guillot P 2020 Investigation of RONS production and complex molecules degradation induced by an APPJ generated by two different sources *IEEE Trans. Radiat. Plasma Med. Sci.* **4** 121–9
- [4] Sousa J S, Niemi K, Cox L J, Th A Q, Gans T and O'Connell D 2011 Cold atmospheric pressure plasma jets as sources of singlet delta oxygen for biomedical applications *J. Appl. Phys.* **109** 123302
- [5] Niemi K, O'Connell D, De Oliveira N, Joyeux D, Nahon L, Booth J P and Gans T 2013 Absolute atomic oxygen and nitrogen densities in radio-frequency driven atmospheric pressure cold plasmas: synchrotron vacuum ultra-violet high-resolution Fourier-transform absorption measurements *Appl. Phys. Lett.* **103** 034102
- [6] Murakami T, Niemi K, Gans T, O'Connell D and Graham W G 2012 Chemical kinetics and reactive species in atmospheric pressure helium–oxygen plasmas with humid-air impurities *Plasma Sources Sci. Technol.* **22** 015003
- [7] Murakami T, Niemi K, Gans T, O'Connell D and Graham W G 2014 Afterglow chemistry of atmospheric-pressure helium–oxygen plasmas with humid air impurity *Plasma Sources Sci. Technol.* **23** 025005
- [8] Dedrick J, Schröter S, Niemi K, Wijaikhum A, Wagenaars E, De Oliveira N, Nahon L, Booth J P, O'Connell D and Gans T 2017 Controlled production of atomic oxygen and nitrogen in a pulsed radio-frequency atmospheric-pressure plasma *J. Phys. D: Appl. Phys.* **50** 455204
- [9] Wijaikhum A, Schröder D, Schröter S, Gibson A R, Niemi K, Friderich J, Greb A, Der Gathen V S, O'Connell D and Gans T 2017 Absolute ozone densities in a radio-frequency driven atmospheric pressure plasma using two-beam UV-LED absorption spectroscopy and numerical simulations *Plasma Sources Sci. Technol.* **26** 115004
- [10] Maletić D, Puač N, Lazović S, Malović G, Gans T, V S D G and Petrović Z L 2012 Detection of atomic oxygen and nitrogen created in a radio-frequency-driven micro-scale atmospheric pressure plasma jet using mass spectrometry *Plasma Phys. Control. Fusion* **54** 124046
- [11] Turner M M 2015 Uncertainty and error in complex plasma chemistry models *Plasma Sources Sci. Technol.* **24** 035027
- [12] Turner M M 2016 Uncertainty and sensitivity analysis in complex plasma chemistry models *Plasma Sources Sci. Technol.* **25** 015003
- [13] Gorbanev Y, O'Connell D and Chechik V 2016 Non-thermal plasma in contact with water: the origin of species *Chem. Eur. J.* **22** 3496–505
- [14] McKay K, Liu D X, Rong M Z, Iza F and Kong M G 2012 Generation and loss of reactive oxygen species in low-temperature atmospheric-pressure RF He + O₂ + H₂O plasmas *J. Phys. D: Appl. Phys.* **45** 172001
- [15] Naidis G V 2014 Production of active species in cold helium–air plasma jets *Plasma Sources Sci. Technol.* **23** 065014

- [16] Reuter S, Tresp H, Wende K, Hammer M U, Winter J, Masur K, Schmidt-Bleker A and Weltmann K-D 2012 From RONS to ROS: tailoring plasma jet treatment of skin cells *IEEE Trans. Plasma Sci.* **40** 2986–93
- [17] Lafleur T, Delattre P A, Johnson E V and Booth J P 2012 Separate control of the ion flux and ion energy in capacitively coupled radio-frequency discharges using voltage waveform tailoring *Appl. Phys. Lett.* **101** 124104
- [18] Bruneau B, Novikova T, Lafleur T, Booth J P and Johnson E V 2014 Control and optimization of the slope asymmetry effect in tailored voltage waveforms for capacitively coupled plasmas *Plasma Sources Sci. Technol.* **24** 015021
- [19] Lommatzsch U, Pasedag D, Baalman A, Ellinghorst G and Wagner H-E 2007 Atmospheric pressure plasma jet treatment of polyethylene surfaces for adhesion improvement *Plasma Processes Polym.* **4** S1041–5
- [20] Shaw D, West A, Bredin J and Wagenaars E 2016 Mechanisms behind surface modification of polypropylene film using an atmospheric-pressure plasma jet *Plasma Sources Sci. Technol.* **25** 065018
- [21] West A, van der Schans M, Xu C, Cooke M and Wagenaars E 2016 Fast, downstream removal of photoresist using reactive oxygen species from the effluent of an atmospheric pressure plasma jet *Plasma Sources Sci. Technol.* **25** 02LT01
- [22] Laroussi M 2005 Low temperature plasma-based sterilization: overview and state-of-the-art *Plasma Process. Polym.* **2** 391–400
- [23] Park G Y, Park S J, Choi M Y, Koo I G, Byun J H, Hong J W, Sim J Y, Collins G J and Lee J K 2012 Atmospheric-pressure plasma sources for biomedical applications *Plasma Sources Sci. Technol.* **21** 043001
- [24] Privat-Maldonado A, O'Connell D, Welch E, Vann R and Van Der Woude M W 2016 Spatial dependence of DNA damage in bacteria due to low-temperature plasma application as assessed at the single cell level *Sci. Rep.* **6** 35646
- [25] Kong M G, Kroesen G, Morfill G, Nosenko T, Shimizu T, van Dijk J and Zimmermann J L 2009 Plasma medicine: an introductory review *New J. Phys.* **11** 115012
- [26] Bekeschus S, Schmidt A, Weltmann K-D and von Woedtke T 2016 The plasma jet kINPen—a powerful tool for wound healing *Clin. Plasma Med.* **4** 19–28
- [27] Isbary G et al 2012 Successful and safe use of 2 min cold atmospheric argon plasma in chronic wounds: results of a randomized controlled trial *Br. J. Dermatol.* **167** 404–10
- [28] Lloyd G, Friedman G, Jafri S, Schultz G, Fridman A and Harding K 2010 Gas plasma: medical uses and developments in wound care *Plasma Process. Polym.* **7** 194–211
- [29] Hirst A M, Simms M S, Mann V M, Maitland N J, O'Connell D and Frame F M 2015 Low-temperature plasma treatment induces DNA damage leading to necrotic cell death in primary prostate epithelial cells *Br. J. Cancer* **112** 1536–45
- [30] Hirst A M, Frame F M, Arya M, Maitland N J and O'Connell D 2016 Low temperature plasmas as emerging cancer therapeutics: the state of play and thoughts for the future *Tumor Biol.* **37** 7021–31
- [31] Gibson A R, McCarthy H O, Ali A A, O'Connell D and Graham W G 2014 Interactions of a non-thermal atmospheric pressure plasma effluent with PC-3 prostate cancer cells *Plasma Processes Polym.* **11** 1142–9
- [32] Vandamme M et al 2012 ROS implication in a new antitumor strategy based on non-thermal plasma *Int. J. Cancer* **130** 2185–94
- [33] Miller H L, Contera S, Wollman A J M, Hirst A, Dunn K E, Schröter S, O'Connell D and Leake M C 2020 Biophysical characterisation of DNA origami nanostructures reveals inaccessibility to intercalation binding sites *Nanotechnology* **31** 235605
- [34] Gorbanev Y, Leifert D, Studer A, O'Connell D and Chechik V 2017 Initiating radical reactions with non-thermal plasmas *Chem. Commun.* **53** 3685–8
- [35] Schüngel E, Korolov I, Bruneau B, Derzsi A, Johnson E, O'Connell D, Gans T, Booth J-P, Donkó Z and Schulze J 2016 Tailored voltage waveform capacitively coupled plasmas in electronegative gases: frequency dependence of asymmetry effects *J. Phys. D: Appl. Phys.* **49** 265203
- [36] Gibson A R, Greb A, Graham W G and Gans T 2015 Tailoring the nonlinear frequency coupling between odd harmonics for the optimisation of charged particle dynamics in capacitively coupled oxygen plasmas *Appl. Phys. Lett.* **106** 054102
- [37] Gibson A R et al 2019 Disrupting the spatio-temporal symmetry of the electron dynamics in atmospheric pressure plasmas by voltage waveform tailoring *Plasma Sources Sci. Technol.* **28** 01LT01
- [38] Locke B R and Shih K-Y 2011 Review of the methods to form hydrogen peroxide in electrical discharge plasma with liquid water *Plasma Sources Sci. Technol.* **20** 034006
- [39] Bekeschus S, Kolata J, Winterbourn C, Kramer A, Turner R, Weltmann K D, Bröker B and Masur K 2014 Hydrogen peroxide: a central player in physical plasma-induced oxidative stress in human blood cells *Free Radic. Res.* **48** 542–9
- [40] Jiang B, Zheng J, Qiu S, Wu M, Zhang Q, Yan Z and Xue Q 2014 Review on electrical discharge plasma technology for wastewater remediation *Chem. Eng. J.* **236** 348–68
- [41] Liu D X, Iza F, Wang X H, Kong M G and Rong M Z 2011 He + O₂ + H₂O plasmas as a source of reactive oxygen species *Appl. Phys. Lett.* **98** 221501
- [42] Liu D-X, Rong M-Z, Wang X-H, Iza F, Kong M G and Bruggeman P 2010 Main species and physicochemical processes in cold atmospheric-pressure He + O₂ plasmas *Plasma Processes Polym.* **7** 846–65
- [43] Gianella M, Reuter S, Press S A, Schmidt-Bleker A, Van Helden J H and Ritchie G A D 2018 HO₂ reaction kinetics in an atmospheric pressure plasma jet determined by cavity ring-down spectroscopy *Plasma Sources Sci. Technol.* **27** 095013
- [44] Knake N, Niemi K, Reuter S, Schulz-von der Gathen V and Winter J 2008 Absolute atomic oxygen density profiles in the discharge core of a microscale atmospheric pressure plasma jet *Appl. Phys. Lett.* **93** 131503
- [45] Niemi K, Reuter S, Graham L M, Waskoenig J and Gans T 2009 Diagnostic based modeling for determining absolute atomic oxygen densities in atmospheric pressure helium-oxygen plasmas *Appl. Phys. Lett.* **95** 151504
- [46] Bruggeman P, Cunge G and Sadeghi N 2012 Absolute OH density measurements by broadband UV absorption in diffuse atmospheric-pressure He–H₂O RF glow discharges *Plasma Sources Sci. Technol.* **21** 035019
- [47] Schröter S et al 2018 Chemical kinetics in an atmospheric pressure helium plasma containing humidity *Phys. Chem. Chem. Phys.* **20** 24263–86
- [48] Waskoenig J, Niemi K, Knake N, Graham L M, Reuter S, Der Gathen V S and Gans T 2010 Atomic oxygen formation in a radio-frequency driven micro-atmospheric pressure plasma jet *Plasma Sources Sci. Technol.* **19** 045018
- [49] Foucher M, Marinov D, Carbone E, Chabert P and Booth J-P 2015 Highly vibrationally excited O₂ molecules in low-pressure inductively-coupled plasmas detected by

- high sensitivity ultra-broad-band optical absorption spectroscopy *Plasma Sources Sci. Technol.* **24** 042001
- [50] Golda J et al 2016 Concepts and characteristics of the ‘COST reference microplasma jet’ *J. Phys. D: Appl. Phys.* **49** 084003
- [51] Dieke G H and Crosswhite H M 1962 The ultraviolet bands of OH Fundamental data *J. Quant. Spectrosc. Radiat. Transfer* **2** 97–199
- [52] Earls L T 1935 Intensities in ${}^2\Pi - {}^2\Sigma$ transitions in diatomic molecules *Phys. Rev.* **48** 423–4
- [53] German K R 1975 Direct measurement of the radiative lifetimes of the $A^2\Sigma^+(V' = 0)$ states of OH and OD *J. Chem. Phys.* **62** 2584–7
- [54] Kasyutich V L 2005 Pressure broadening parameters of the hydroxyl radical $A^2\Sigma^+(v' = 0) \leftarrow X^2\Pi_{3/2}(v = 0)$ transitions at ca. 308 nm *Eur. Phys. J. D* **33** 29–33
- [55] Lietz A M and Kushner M J 2016 Air plasma treatment of liquid covered tissue: long timescale chemistry *J. Phys. D: Appl. Phys.* **49** 425204
- [56] Bruggeman P and Schram D C 2010 On OH production in water containing atmospheric pressure plasmas *Plasma Sources Sci. Technol.* **19** 045025
- [57] Naidis G V 2013 Modelling of OH production in cold atmospheric-pressure He–H₂O plasma jets *Plasma Sources Sci. Technol.* **22** 035015
- [58] Schröter S, Bredin J, Gibson A R, West A, Dedrick J P, Wagenaar E, Niemi K, Gans T and O’Connell D 2020 The formation of atomic oxygen and hydrogen in atmospheric pressure plasmas containing humidity: picosecond two-photon absorption laser induced fluorescence and numerical simulations *Plasma Sources Sci. Technol.* **29** 105001
- [59] Ono R and Tokuhiro M 2020 Spatiotemporal measurement of OH density from upstream to downstream in humid helium atmospheric-pressure plasma jet *Plasma Sources Sci. Technol.* **29** 035021
- [60] Biagi v8.9 database (available at: www.lxcat.net) (Accessed 29 July 2020) retrieved July 2012
- [61] Biagi S F Fortran program, MAGBOLTZ, versions 8.9 and after (www.lxcat.net/Biagi)
- [62] Itikawa Y and Mason N 2005 Cross sections for electron collisions with water molecules *J. Phys. Chem. Ref. Data* **34** 1–22
- [63] Yousfi M and Benabdessadok M D 1996 Boltzmann equation analysis of electron-molecule collision cross sections in water vapor and ammonia *J. Appl. Phys.* **80** 6619–30
- [64] Lawton S A and Phelps A V 1978 Excitation of the $b^1\Sigma_g^+$ state of O₂ by low energy electrons *J. Chem. Phys.* **69** 1055–68
- [65] Vriens L 1964 Calculation of absolute ionisation cross sections of He, He*, He⁺, Ne, Ne*, Ne⁺, Ar, Ar*, Hg and Hg* *Phys. Lett.* **8** 260–1
- [66] Flannery M R, McCann K J and Winter N W 1981 Cross sections for electron impact ionisation of metastable rare-gas excimers (He₂^{*}, Kr₂^{*}, Xe₂^{*}) *J. Phys. B: At. Mol. Opt. Phys.* **14** 3789–96
- [67] Riahi R, Teulet P, Lakhdar Z B and Gleizes A 2006 Cross-section and rate coefficient calculation for electron impact excitation, ionisation and dissociation of H₂ and OH molecules *Eur. Phys. J. D* **40** 223–30
- [68] Laher R R and Gilmore F R 1990 Updated excitation and ionization cross sections for electron impact on atomic oxygen *J. Phys. Chem. Ref. Data* **19** 277–305
- [69] Gryziński M 1965 Classical theory of atomic collisions. I. Theory of inelastic collisions *Phys. Rev.* **138** A336–58
- [70] Hall R I and Trajmar S 1975 Scattering of 4.5 eV electrons by ground ($X^3\Sigma_g^-$) state and metastable ($a^1\Delta_g$) oxygen molecules *J. Phys. B: At. Mol. Opt. Phys.* **8** L293–6
- [71] Josphipura K N, Antony B K and Vinodkumar M 2002 Electron scattering and ionization of ozone, O₂ and O₄ molecules *J. Phys. B: At. Mol. Opt. Phys.* **35** 4211–21
- [72] McConkey J, Malone C, Johnson P, Winstead C, McKoy V and Kanik I 2008 Electron impact dissociation of oxygen-containing molecules—A critical review *Physics Reports Phys. Rep.* **466** 1–103
- [73] Deloche R, Monchicourt P, Cheret M and Lambert F 1976 High-pressure helium afterglow at room temperature *Phys. Rev. A* **13** 1140–76
- [74] Kedzierski W, Derbyshire J, Malone C and McConkey J W 1998 Isotope effects in the electron impact break-up of water *J. Phys. B: At. Mol. Opt. Phys.* **31** 5361–8
- [75] Harb T, Kedzierski W and McConkey J W 2001 Production of ground state OH following electron impact on H₂O *J. Chem. Phys.* **115** 5507–12
- [76] Ding K, Lieberman M A and Lichtenberg A J 2014 Hybrid model of neutral diffusion, sheaths, and the alpha to gamma transition in an atmospheric pressure He/H₂O bounded rf discharge *J. Phys. D: Appl. Phys.* **47** 305203
- [77] Corrigan S J B 1965 Dissociation of molecular hydrogen by electron impact *J. Chem. Phys.* **43** 4381–6
- [78] Hayashi M 1979 Monte Carlo simulation of electron avalanche in hydrogen *J. Phys. Colloq.* **40** C7-45–C7-46
- [79] W Liu and G A Victor 1994 Electron Energy Deposition in Carbon Monoxide Gas *Astrophys. J.* **435** 909
- [80] Soloshenko I A, Tsiolko V V, Pogulay S S, Kalyuzhnaya A G, Bazhenov V Y and Shchedrin A I 2009 Effect of water adding on kinetics of barrier discharge in air *Plasma Sources Sci. Technol.* **18** 045019
- [81] Gupta M and Baluja K L 2005 Electron collisions with an ozone molecule using the R-matrix method *J. Phys. B: At. Mol. Opt. Phys.* **38** 4057–73
- [82] Krishnakumar E and Srivastava S 1992 Cross-sections for electron impact ionization of O₂ *Int. J. Mass Spectrometry and Ion Processes* **113** 1–12
- [83] Melton C E and Neece G A 1971 Rate constants and cross sections for the production of OH⁻ from O⁻ and H⁻ in water *J. Am. Chem. Soc.* **93** 6757–9
- [84] Nandi D, Krishnakumar E, Rosa A, Schmidt W-F and Illenberger E 2003 Dissociative electron attachment to H₂O₂: a very effective source for OH and OH⁻ generation *Chem. Phys. Lett.* **373** 454–9
- [85] Burrow P D 1973 Dissociative attachment from the O₂($a^1\Delta_g$) state *J. Chem. Phys.* **59** 4922–31
- [86] Matejčík S, Kiendler A, Cicman P, Skalný J, Stampfli P, Illenberger E, Chu Y, Stamatovic A and Märk T D 1997 Electron attachment to molecules and clusters of atmospheric relevance: oxygen and ozone *Plasma Sources Sci. Technol.* **6** 140–6
- [87] Janev R K, Langer W D, Evans K J and Post D E J 1987 *Elementary Processes in Hydrogen-Helium Plasmas: Cross Sections and Reaction Rate Coefficients* (Berlin: Springer)
- [88] Pedersen H B, Djurić N, Jensen M J, Kella D, Safvan C P, Schmidt H T, Vejby-Christensen L and Andersen L H 1999 Electron collisions with diatomic anions *Phys. Rev. A* **60** 2882–99
- [89] Deutsch H, Scheier P, Becker K and Märk T D 2003 Calculated cross-sections for the electron-impact detachment from negative ions using the Deutsch–Märk (DM) formalism *Chem. Phys. Lett.* **382** 26–31

- [90] Deutsch H, Becker K, Probst M, Zhu W and Märk T 2008 Calculated absolute cross-sections for the electron-induced detachment of the B_2^- , O_2^- , BO^- , and CN^- anions using the Deutsch-Märk (DM) formalism *Int. J. Mass Spectrometry* **277** 151–4
- [91] Seiersen K, Bak J, Bluhme H, Jensen M J, Nielsen S B and Andersen L H 2003 Electron-impact detachment of O_3^- , NO_3^- and SO_2^- ions *Phys. Chem. Chem. Phys.* **5** 4814–20
- [92] M A Biondi 1976 chapter 4 Principles of Laser Plasmas Wiley (New York: G Bekefi)
- [93] Florescu-Mitchell A I and Mitchell J B A 2006 Dissociative recombination *Phys. Rep.* **430** 277–374
- [94] McElroy D, Walsh C, Markwick A J, Cordiner M A, Smith K and Millar T J 2013 The UMIST database for astrochemistry 2012 *Astron. Astrophys.* **550** A36
- [95] Rosén S et al 2000 Recombination of simple molecular ions studied in storage ring: dissociative recombination of H_2O^+ *Faraday Discuss.* **115** 295–302
- [96] Jensen M J, Bilodeau R C, Safvan C P, Seiersen K, Andersen L H, Pedersen H B and Heber O 2000 Dissociative Recombination of H_3O^+ , HD_2O^+ , and D_3O^+ *Astrophys. J.* **543** 764–74
- [97] Novotný O et al 2010 Fragmentation channels in dissociative electron recombination with hydronium and other astrophysically important species *J. Phys. Chem. A* **114** 4870–4
- [98] Bortner M H and Baurer T 1978 *Defense Nuclear Agency Reaction Rate Handbook Second Revision Number 7* (Philadelphia, PA: Space Div., General Electric Co.)
- [99] Huang C-M, Whitaker M, Biondi M A and Johnsen R 1978 Electron-temperature dependence of recombination of electrons with H_3O^+ . (H_2O) n -series ions *Phys. Rev. A* **18** 64–67
- [100] Leu M T, Biondi M A and Johnsen R 1973 Measurements of the recombination of electrons with H_3O^+ . (H_2O) n -Series Ions *Phys. Rev. A* **7** 292–8
- [101] Peverall R et al 2001 Dissociative recombination and excitation of O_2^+ : cross sections, product yields and implications for studies of ionospheric airglows *J. Chem. Phys.* **114** 6679–89
- [102] Zhaunerchyk V, Geppert W D, Österdahl F, Larsson M, Thomas R D, Bahati E, Bannister M E, Fogle M R and Vane C R 2008 Dissociative recombination dynamics of the ozone cation *Phys. Rev. A* **77**
- [103] Dulaney J L, Biondi M A and Johnsen R 1988 Electron-temperature dependence of the recombination of electrons with O_4^+ ions *Phys. Rev. A* **37** 2539–42
- [104] Hagelaar G J M and Pitchford L C 2005 Solving the Boltzmann equation to obtain electron transport coefficients and rate coefficients for fluid models *Plasma Sources Sci. Technol.* **14** 722
- [105] Morgan (Kinema Research & Software) database (available at: www.lxcat.net)
- [106] Kossyi I A, Kostinsky A Y, Matveyev A A and Silakov V P 1992 Kinetic scheme of the non-equilibrium discharge in nitrogen-oxygen mixtures *Plasma Sources Sci. Technol.* **1** 207–20
- [107] Prasad S S and Huntress W T, Jr 1980 A model for gas phase chemistry in interstellar clouds: I. The basic model, library of chemical reactions, and chemistry among C, N, and O compounds *Astrophys. J. Suppl. Ser.* **43** 1–35
- [108] Mauclaire G, Derai R and Marx R 1978 ICR determination of kinetically excited ions produced in water and methane by charge transfer from thermal rare gas ions *Int. J. Mass Spectrom. Ion Phys.* **26** 289–301
- [109] Eichelberger B R, Snow T P and Bierbaum V M 2003 Collision rate constants for polarizable ions *J. Am. Soc. Mass Spectrom.* **14** 501–5
- [110] Langevin M P 1905 Une formule fondamentale de theorie cinetique *Annales De Chimie Et De Physique, Series* **5** 245–88
- [111] Miller T M 2000 Atomic and molecular polarizabilities *CRC Handbook of Chemistry and Physics* vol 77 (Boca Raton, FL: CRC Press) pp 193–202
- [112] Adams N G and Smith D 1976 Product-ion distributions for some ion-molecule reactions *J. Phys. B: At. Mol. Opt. Phys.* **9** 1439–51
- [113] Ikezoe Y 1987 *Gas Phase Ion-molecule Reaction Rate Constants through 1986* (Ion Reaction Research Group of the Mass Spectroscopy Society of Japan) (<http://www.mssj.jp/english/publications/books.html>)
- [114] Jones J D C, Birkinshaw K and Twiddy N D 1981 Rate coefficients and product ion distributions for the reactions of OH^+ and H_2O^+ with N_2 , O_2 , NO , N_2O , Xe , CO , CO_2 , H_2S and H_2 at 300 K *Chem. Phys. Lett.* **77** 484–8
- [115] Huntress W T and Pinizzotto R F 1973 Product distributions and rate constants for ion-molecule reactions in water, hydrogen sulfide, ammonia, and methane *J. Chem. Phys.* **59** 4742–56
- [116] Rakshit A B and Warneck P 1980 Reactions of CO_2^+ , $CO_2CO_2^+$ and H_2O^+ ions with various neutral molecules *J. Chem. Soc. Faraday Trans.* **76** 1084–92
- [117] Viggiano A A, Albritton D L, Fehsenfeld F C, Adams N G, Smith D and Howorka F 1980 Laboratory studies of some ion-atom reactions related to interstellar molecular synthesis *Astrophys. J.* **236** 492–7
- [118] Anicich V G 1993 Evaluated bimolecular ion-molecule gas phase kinetics of positive ions for use in modeling planetary atmospheres, cometary comae, and interstellar clouds *J. Phys. Chemical Ref. Data* **22** 1469–569
- [119] Sieck L W, Heron J T and Green D S 2000 Chemical kinetics database and predictive schemes for humid air plasma chemistry. Part I: positive ion-molecule reactions *Plasma Chem. Plasma Process.* **20** 235–58
- [120] Smith D, Adams N G and Miller T M 1978 A laboratory study of the reactions of N^+ , N_2^+ , N_3^+ , N_4^+ , O^+ , O_2^+ , and NO^+ ions with several molecules at 300 K *J. Chem. Phys.* **69** 308–18
- [121] McFarland M, Albritton D L, Fehsenfeld F C, Ferguson E E and Schmeltekopf A L 1973 Flow-drift technique for ion mobility and ion-molecule reaction rate constant measurements. II. Positive ion reactions of N^+ , O^+ , and H_2^+ with O_2 and O^+ with N_2 from thermal to “2 eV *J. Chem. Phys.* **59** 6620–8
- [122] Crosby D A and Zorn J C 1977 Dipole polarizability of 2^3S_1 and 2^1S_0 metastable helium measured by the electric deflection time-of-flight method *Phys. Rev. A* **16** 488–91
- [123] de Petris G 2003 Atmospherically relevant ion chemistry of ozone and its cation *Mass Spectrom. Rev.* **22** 251–71
- [124] Rakshit A B and Warneck P 1980 A drift chamber study of the formation of water cluster ions in oxygen *J. Chem. Phys.* **73** 5074–80
- [125] Nesbet R K 1977 Atomic polarizabilities for ground and excited states of C, N, and O *Phys. Rev. A* **16** 1–5
- [126] Champion R L, Doverspike L D and Lam S K 1976 Electron detachment from negative ions: the effects of isotopic substitution *Phys. Rev. A* **13** 617–21
- [127] Bruhns H, Kreckel H, Miller K A, Urbain X and Savin D W 2010 Absolute energy-resolved measurements of the $H^+ + H \rightarrow H_2 + e^-$ associative detachment reaction using a merged-beam apparatus *Phys. Rev. A* **82** 042708
- [128] Martinez O, Yang Z, Demarais N J, Snow T P and Bierbaum V M 2010 Gas-phase reactions of hydride anion, H^- *Astrophys. J.* **720** 173–7

- [129] Ferguson E E 1973 Rate constants of thermal energy binary ion-molecule reactions of aeronomic interest *Atomic Data and Nuclear Data Tables* **12** 159–78
- [130] Fehsenfeld F C and Ferguson E E 1974 Laboratory studies of negative ion reactions with atmospheric trace constituents *J. Chem. Phys.* **61** 3181–93
- [131] Penent F, Grouard J P, Hall R I, Montmagnon J L, Champion R L, Doverspike L D and Esaulov V A 1987 Fundamental processes in collisions of O^- with atoms and molecules; mechanisms of one- and two-electron loss *J. Phys. B: At. Mol. Phys.* **20** 6065
- [132] Belostotsky S G, Economou D J, Lopaev D V and Rakhimova T V 2005 Negative ion destruction by $O(^3P)$ atoms and $O_2(a^1\Delta_g)$ molecules in an oxygen plasma *Plasma Sources Sci. Technol.* **14** 532
- [133] Ard S G, Melko J J, Jiang B, Li Y, Shuman N S, Guo H and Viggiano A A 2013 Temperature dependences for the reactions of O_2^- and O^- with N and O atoms in a selected-ion flow tube instrument *J. Chem. Phys.* **139** 144302
- [134] Midey A, Dotan I and Viggiano A A 2008 Temperature Dependences for the Reactions of O^- and O_2^- with $O_2(a\Delta_g)$ from 200 to 700 K *J. Phys. Chem. A* **112** 3040–5
- [135] Lifshitz C, Wu R L C, Haartz J C and Tiernan T O 1977 Associative detachment reactions of negative ions with O_3 *J. Chem. Phys.* **67** 2381–2
- [136] Axford S D T and Hayhurst A N 1996 Mass spectrometric sampling of negative ions from flames of hydrogen and oxygen: the kinetics of electron attachment and detachment in hot mixtures of H_2O , O_2 , OH and HO_2 *Proc. R. Soc. A* **452** 1007–33
- [137] Bohringer H, Glebe W and Arnold F 1983 Temperature dependence of the mobility and association rate coefficient of He^+ ions in He from 30–350K *J. Phys. B: At. Mol. Opt. Phys.* **16** 2619–26
- [138] Lau Y K, Ikuta S and Kebarle P 1982 Thermodynamics and kinetics of the gas-phase reactions $H_3O^+(H_2O)_{n-1} + \text{water} = H_3O^+(H_2O)_n$ *J. Am. Chem. Soc.* **104** 1462–9
- [139] Böhringer H, Arnold F, Smith D and Adams N 1983 A study of the temperature dependences of the $N_2^+ + N_2 \rightarrow N_4^+$ and $O_2^+ + O_2 \rightarrow O_4^+$ association reactions using the selected-ion flow-tube and drift-tube techniques *Int. J. Mass Spectrometry and Ion Phys.* **52** 25–41
- [140] de Urquijo J, Bekstein A, Ruiz-Vargas G and Gordillo-Vázquez F J 2012 Drift and clustering of daughter negative ions of H_2O in parent gas *J. Phys. D: Appl. Phys.* **46** 035201
- [141] Johnston H S 1968 *Gas phase reaction kinetics of neutral oxygen species Technical Report NSRDS-NBS-20*, National Bureau of Standards (National Standard Reference Data System) (<https://apps.dtic.mil/sti/citations/ADD095263>)
- [142] Heidner R F and Husain D 1974 A study of the collisional quenching of $O(2^1D_2)$ by the noble gases employing time-resolved attenuation of atomic resonance radiation in the vacuum ultraviolet *Int. J. Chem. Kinet.* **6** 77–87
- [143] Becker K H, Groth W and Schurath U 1971 The quenching of metastable $O_2(^1\Delta_g)$ and $O_2(^1\Sigma_g^+)$ molecules *Chem. Phys. Lett.* **8** 259–62
- [144] Stafford D S and Kushner M J 2004 $O_2(^1\Delta)$ production in He/O_2 mixtures in flowing low pressure plasmas *J. Appl. Phys.* **96** 2451–65
- [145] Niemi K, Waskoenig J, Sadeghi N, Gans T and O'Connell D 2011 The role of helium metastable states in radio-frequency driven helium–oxygen atmospheric pressure plasma jets: measurement and numerical simulation *Plasma Sources Sci. Technol.* **20** 055005
- [146] Collins C B and Lee F W 1979 Measurement of the rate coefficients for the bimolecular and termolecular de-excitation reactions of $He(2^3S)$ with selected atomic and molecular species *J. Chem. Phys.* **70** 1275–85
- [147] Sanders R A and Muschlitz E E 1977 Chemiionization and secondary ion reactions in H_2O and D_2O *Int. J. Mass Spectrom. Ion Phys.* **23** 99–108
- [148] Pouvesle J M, Khacef A, Stevefelt J, Jahani H, Gylys V T and Collins C B 1988 Study of two-body and three-body channels for the reaction of metastable helium atoms with selected atomic and molecular species *J. Chem. Phys.* **88** 3061–71
- [149] Phelps A V and Molnar J P 1953 Lifetimes of metastable states of noble gases *Phys. Rev.* **89** 1202–8
- [150] Pouvesle J M, Stevefelt J, Lee F W, Jahani H R, Gylys V T and Collins C B 1985 Reactivity of metastable helium molecules in atmospheric pressure afterglows *J. Chem. Phys.* **83** 2836–9
- [151] Tsang W and Hampson R F 1986 Chemical kinetic data base for combustion chemistry. Part I. Methane and related compounds *J. Phys. Chem. Ref. Data* **15** 1087–279
- [152] Atkinson R, Baulch D L, Cox R A, Crowley J N, Hampson R F, Hynes R G, Jenkin M E, Rossi M J and Troe J 2004 Evaluated kinetic and photochemical data for atmospheric chemistry: volume I—gas phase reactions of O_x , HO_x , NO_x and SO_x species *Atmos. Chem. Phys.* **4** 1461–738
- [153] Baulch D L et al 1992 Evaluated kinetic data for combustion modelling *J. Phys. Chem. Ref. Data* **21** 411–734
- [154] Burkholder J B, Sander S P, Abbatt J P D, Barker J R, Huie R E, Kolb C E, Kurylo M J, Orkin V L, Wilmouth D M and Wine P H 2015 *Chemical Kinetics and Photochemical Data for Use in Atmospheric Studies: Evaluation Number 18* (Pasadena, CA: Jet Propulsion Laboratory, National Aeronautics and Space Administration)
- [155] Manion J A et al 2015 NIST chemical kinetics database web version 7.0 (available at: <https://kinetics.nist.gov/>)
- [156] Orkin V L, Kozlov S N, Poskrebyshv G A and Kurylo M J 2006 Rate constant for the reaction of OH with H_2 between 200 and 480 K *J. Phys. Chem. A* **110** 6978–85
- [157] Baulch D L et al 2005 Evaluated kinetic data for combustion modeling: supplement II *J. Phys. Chem. Ref. Data* **34** 757–1397
- [158] Keyser L F 1988 Kinetics of the reaction $OH + HO_2 \rightarrow H_2O + O_2$ from 254 to 382 K *J. Phys. Chem.* **92** 1193–200
- [159] Lewis R S and Watson R T 1980 Temperature dependence of the reaction $O(3P) + OH(2II) \rightarrow O_2 + H$ *J. Phys. Chem.* **84** 3495–503
- [160] Howard M J and Smith I W M 1981 Direct rate measurements on the reactions $N + OH \rightarrow NO + H$ and $O + OH \rightarrow O_2 + H$ from 250 to 515 K *J. Chem. Soc. Faraday Trans.* **77** 997–1008
- [161] Slinger T G and Black G 1978 $O(^1S)$ interactions—the product channels *J. Chem. Phys.* **68** 989–97
- [162] Fletcher I S and Husain D 1976 The collisional quenching of electronically excited oxygen atoms, $O(2^1D_2)$, by the gases NH_3 , H_2O_2 , C_2H_6 , C_3H_8 , and $C(CH_3)_4$, using time-resolved attenuation of atomic resonance radiation *Can. J. Chem.* **54** 1765–70
- [163] Abreu V J, Yee J H, Solomon S C and Dalgarno A 1986 The quenching rate of $O(^1D)$ by $O(^3P)$ *Planet. Space Sci.* **34** 1143–5

- [164] Schofield K 1978 Rate constants for the gaseous interaction of $O(2^1D_2)$ and $O(2^1S_0)$ —a critical evaluation *J. Photochem.* **9** 55–68
- [165] Wine P H, Nicovich J M, Thompson R J and Ravishankara A R 1983 Kinetics of atomic oxygen(3PJ) reactions with hydrogen peroxide and ozone *J. Phys. Chem.* **87** 3948–54
- [166] Slanger T G and Black G 1981 The product channels in the quenching of $O(^1S)$ by $O_2(a^1\Delta_g)$ *J. Chem. Phys.* **75** 2247–51
- [167] Slanger T G and Black G 1981 Quenching of $O(^1S)$ by $O_2(a^1D_g)$ *Geophys. Res. Lett.* **8** 535–8
- [168] Kenner R D and Ogryzlo E A 1982 A direct determination of the rate constant for the quenching of $O(^1S)$ by $O_2(a^1\Delta_g)$ *J. Photochem.* **18** 379–82
- [169] Steinfeld J I, Adler-Golden S M and Gallagher J W 1987 Critical survey of data on the spectroscopy and kinetics of ozone in the mesosphere and thermosphere *J. Phys. Chem. Ref. Data* **16** 911–51
- [170] Derwent G R and Thrush B A 1971 Measurements on $O_2^1\Delta_g$ and $O_2^1\Sigma^+_g$ in discharge flow systems *Trans. Faraday Soc.* **67** 2036–43
- [171] Heidner R F, Gardner C E, El-Sayed T M, Segal G I and Kasper J V V 1981 Temperature dependence of $O_2(^1\Delta)+O_2(^1\Delta)$ and $I(^2P_{1/2})+O_2(^1\Delta)$ energy pooling *J. Chem. Phys.* **74** 5618–26
- [172] Myers G and Cunningham A J 1977 Rate measurements of reactions of helium metastable species at atmospheric pressures. I. He (2^3S) in pure afterglows *J. Chem. Phys.* **67** 247–53
- [173] Manion J A et al NIST chemical kinetics database NIST Standard Reference Database 17, Version 7.0 (Web Version), Release 1.6.8, Data version 2015.12. National Institute of Standards and Technology, Gaithersburg, Maryland, 20899–8320 (<http://kinetics.nist.gov/>)
- [174] Sellevåg S R, Georgievskii Y and Miller J A 2008 The temperature and pressure dependence of the reactions $H + O_2 (+M) \rightarrow HO_2 (+M)$ and $H + OH (+M) \rightarrow H_2O (+M)$ *J. Phys. Chem. A* **112** 5085–95
- [175] Zellner R, Erler K and Field D 1977 Kinetics of the recombination reaction $OH + H + M \rightarrow H_2O + M$ at low temperatures *Symp. (Int.) on Combustion* vol **16** pp 939–48
- [176] Hsu K-J, Durant J L and Kaufman F 1987 Rate constants for $H + O_2 + M$ at 298 K for $M = He, N_2,$ and H_2O *J. Phys. Chem.* **91** 1895–9
- [177] Slanger T G and Copeland R A 2003 Energetic oxygen in the upper atmosphere and the laboratory *Chem. Rev.* **103** 4731–66
- [178] Lin C L and Leu M T 1982 Temperature and third-body dependence of the rate constant for the reaction $O + O_2 + M \rightarrow O_3 + M$ *Int. J. Chem. Kinet.* **14** 417–34
- [179] Azyazov V N, Mikheyev P, Postell D and Heaven M C 2009 $O_2(a^1\Delta)$ quenching in the $O/O_2/O_3$ system *Chem. Phys. Lett.* **482** 56–61
- [180] Braginskiy O V, Vasilieva A N, Klopovskiy K S, Kovalev A S, Lopaev D V, Proshina O V, Rakhimova T V and Rakhimov A T 2005 Singlet oxygen generation in O_2 flow excited by RF discharge: I. Homogeneous discharge mode: alpha-mode *J. Phys. D: Appl. Phys.* **38** 3609–25
- [181] Forster R, Frost M, Fulle D, Hamann H F, Hippler H, Schlegel A and Troe J 1995 High pressure range of the addition of HO to HO, NO, NO_2 , and CO. I. Saturated laser induced fluorescence measurements at 298 K *J. Chem. Phys.* **103** 2949–58
- [182] Fulle D, Hamann H F, Hippler H and Troe J 1996 High-pressure range of the addition of HO to HO. III. Saturated laser-induced fluorescence measurements between 200 and 700 K *J. Chem. Phys.* **105** 1001–6